Peter Pichler, BSc.

Non-equilibrium transport calculations:

The variational cluster approximation

MASTER'S THESIS

to achieve the university degree of

Diplom-Ingenieur

Master's degree programme: Technical Physics

submitted to

Graz University of Technology

Supervisor

Univ.-Prof. Dipl.-Phys. Dr.rer.nat. Wolfgang von der Linden

Institute of Theoretical Physics - Computational Physics, TU Graz

Graz, May 2017

AFFIDAVIT

I declare that I have authored this thesis independently, that I have not used other than the declared sources/resources, and that I have explicitly indicated all material which has been quoted either literally or by content from the sources used. The text document uploaded to TUGRAZonline is identical to the present master‘s thesis.

Date

Signature

Abstract

Cluster perturbation methods are a viable tool in dealing with non-equilibrium calculations on large models. It is the main goal of this thesis to study such methods, by applying them on a suitable model. Therefore a finite one-dimensional tight-binding Hubbard-chain was the model of choice. At first, the system was analyzed thoroughly, using cluster perturbation theory. Fermionic bath chains were attached to the thight-binding chain, to obtain a dissipation mechanism to surpress occurring Bloch-oscillations. Driven out of equilibrium by an external electric field, the current through the tight-binding chain was calculated for different interaction parameters, according to the Hubbard-model.

Finally the variational cluster approximation was introduced, by adding auxilary bath sites to the central region. The alteration of the self-energy leads to a different behaviour at non-zero interaction parameters. The variational parameters used, were the on-site energy of the auxiliary bath sites as well as the hopping strength into these bath sites.

Acknowledgements

Thank you, Prof. Wolfgang von der Linden, for your guidance and support throughout the creation of this master thesis. Your sympathic and patient way of explaining anything that was not clear to me made this work possible…

Thank you, Mama and Papa, for your moral and financial support, a loving and caring childhood and being there for me in every possible way, throughout school and university. I would not have come this far without you.…

Thank you, Jakob for your help in the early and later stages of this work. Hours and hours we spent at my computer, discussing the used methods and looking for errors. Thank you for your time, patience and support…

Thank you, Prof. Enrico Arrigoni, Delia, Irakli, Antonius, Max and Gerhard, for the discussions and foods for thought…

Thank you, Peter and Michael! It was great working around you and being able to talk to you about many different topics, during work as well as during the occasional coffee breaks…

Contents

List of Figures

List of Abbreviations

CPT	**C**luster **P**erturbation **T**heory
ED	**E**xact **D**iagonalization
VCA	**V**ariational **C**luster **A**pproximation
KNEGF	**K**eldysh **N**on **E**quilibrium **G**reenfunction **F**ormalism
GF	**G**reen **F**unction
SFT	**S**elf-energy **F**unctional **T**heory

Chapter 1

Introduction

The treatment of large correlated systems in non-equilibrium conditions has been one of the most studied topics of many-body physics for the past decades. The development of numerical techniques to solve such systems is a foundation to the understanding of all kinds of materials and mechanisms like magnetism and super-conductivity.
However, before it is possible to solve macroscopic systems, like a solid block of metal, these numerical techniques have to be tested and further developed on small systems. Common models like the one-dimensional Hubbard model provide solvable systems, which gives a good description of experimentally found behaviours.
The specific numerical method to treat systems like the Hubbard model used in this thesis is the cluster perturbation theory and especially the improved version of it, the variational cluster approximation. As already mentioned, a one-dimensional Hubbard model will be investigated. The thesis is restricted on a finite system of a tight-binding model, populated by electrons, and spinless fermions in the last chapter.
In this first chapter, a brief overview of the most important methods used in this thesis, is given. In chapter 2 the electronic transport through a finite tight-binding chain is analysed, using CPT. In chapter 3 the variational cluster approximation is introduced and applied to the tight-binding chain. The final chapter deals with spinless fermions, inhabiting a quantum dot.

1.1 Green Function formalism

1.1.1 Introduction

One of the main interests of the quantum mechanical approach to many-body physics is to understand a physical system in terms of quantities that are experimentally observable. The measured variables of interest are

1. The eigenvalues of observables
2. The expectation values of observables $\left\langle \hat{A}(t) \right\rangle, \left\langle \hat{B}(t) \right\rangle, ...$
3. The correlation function between observables $\left\langle \hat{A}(t) \cdot \hat{B}(t) \right\rangle ...$

With the methods of statistical mechanics the calculation of measured variables of the types 2 and 3 is possible if the partition function of the system has to

be known, which requires the knowledge of the eigenvalues and eigenstates of the Hamilton-operator. In the case of many-body-calculations, the calculations of those can, in general, not be taken as granted. The **method of Green functions** gives a, in most cases, approximated calculation of correlation functions and expectation values, without the knowledge of the partition function of the system. [30]
The connection of a Green function to an experiment, as sketched briefly in [9] is the following: One considers an experiment, where the system is put under the influence of a disturbance, controlled by an external field $\mathcal{F}(\mathbf{r}, t)$. It is spoken of a linear response if the response depends linear on the perturbation, which is the case if the applied field $\mathcal{F}(\mathbf{r}, t)$ is weak. The given system can be described by the Hamilton operator

$$H = H_0 + V \tag{1.1}$$

with H_0 being the Hamiltonian of the unperturbated system and V the perturbation term. The external field shall be coupled with observable $\hat{B}$:

$$V = \hat{B}\mathcal{F}(t) \tag{1.2}$$

where now only the time dependence of the field is considered.
Further $\hat{A}$ is a not explicit time dependent observable with expectation value $\left\langle \hat{A} \right\rangle$.
It is of interest how $\left\langle \hat{A} \right\rangle$ reacts to a perturbation V.
Following [30] we find the reaction of the system to perturbation V to be

$$\Delta A_t = \left\langle \hat{A} \right\rangle_t - \left\langle \hat{A} \right\rangle_0 = -\frac{i}{\hbar} \int_{-\infty}^{t} dt' \mathcal{F}(t') \, \langle [\, \hat{A}^D(t), \hat{B}^D(t') \,]_- \rangle_0 \tag{1.3}$$

with the two operators in the Dirac picture. We now define the

RETARDED GREEN FUNCTION

$$G^{ret}_{AB}(t, t') = \langle\langle \, A(t); B(t') \, \rangle\rangle^{ret} = -i\Theta(t - t') \, \langle [\, \hat{A}(t), \hat{B}(t') \,]_- \rangle_0 \, . \tag{1.4}$$

Types of Green functions Giving only the retarded Green function is not sufficient for the full Green function formalism. In fact, two more functions need to be defined:

ADVANCED GREEN FUNCTION

$$G^{av}_{AB}(t,t') = \langle\langle\, A(t); B(t')\,\rangle\rangle^{av} = +i\Theta(t-t')\,\langle[\,\hat{A}(t),\hat{B}(t')\,]_-\rangle_0 \tag{1.5}$$

CAUSAL GREEN FUNCTION

$$G^{c}_{AB}(t,t') = \langle\langle\, A(t); B(t')\,\rangle\rangle^{c} = -i\,\langle T_\epsilon\,(A(t)B(t'))\rangle \tag{1.6}$$

T_ϵ is Wick's time-order operator that sorts operators after their time arguments:

$$T_\epsilon\,(A(t)B(t')) = \Theta(t-t')A(t)Bt') + \epsilon\Theta(t'-t)B(t')A(t). \tag{1.7}$$

There are other types of Green functions like the important **Keldysh Green function**, which will be discussed later in this thesis.

1.1.2 The Lehmann represantation of the Green function

As shown in [38] once the groundstate of a Hamiltonian H is known, the zero-temperature Green function $G_{\mu\nu}(\omega)$ can be expressed as

$$\begin{aligned} G'_{\mu\nu}(\omega) &= G'_{\mu\nu,e}(\omega) + G'_{\mu\nu,h}(\omega) && (1.8)\\ G'_{\mu\nu,e}(\omega) &= \langle\Omega|\, c_\mu \frac{1}{\omega - H + E_0}\,|\Omega\rangle && (1.9)\\ G'_{\mu\nu,h}(\omega) &= \langle\Omega|\, c_\mu \frac{1}{\omega + H - E_0}\,|\Omega\rangle && (1.10) \end{aligned}$$

with Ω the groundstate and E_0 the groundstate energy. Inserting completeness relations gives

$$G'_{\mu\nu}(\omega) = \sum_m \langle\Omega|\, c_\mu\,|m\rangle \frac{1}{\omega - H + E_0} \langle m|\, c^\dagger_\nu\,|\Omega\rangle + \sum_n \langle\Omega|\, c^\dagger_\nu\,|\Omega\rangle \frac{1}{\omega + H - E_0} \langle n|\, c_\mu\,|\Omega\rangle \tag{1.11}$$

$\mu = (\mathbf{R}, \sigma)$ concludes both the site as well as the spin. Now one can introduce a further notation to simplify this expression:

$$
\begin{aligned}
Q^{(e)}_{\mu m} &= \langle \Omega | \, c_\mu \, | m \rangle && (1.12)\\
Q^{(h)}_{\nu n} &= \langle \Omega | \, c^\dagger_\nu \, | n \rangle && (1.13)\\
\omega^e_m &= E_m - E_0 && (1.14)\\
\omega^h_n &= E_0 - E_n, && (1.15)
\end{aligned}
$$

which leads to

$$G'_{\mu\nu}(\omega) = \sum_m \frac{Q^{(e)}_{\mu m} Q^{(e)*}_{\nu m}}{\omega - \omega^e_m} + \sum_n \frac{Q^{(h)}_{\mu n} Q^{(h)*}_{\nu n}}{\omega - \omega^h_n} \tag{1.16}$$

Building up matrices

$$\mathbf{Q} = \begin{pmatrix} \mathbf{Q}^{(e)} \\ \mathbf{Q}^{(h)} \end{pmatrix} \tag{1.17}$$

and

$$\mathbf{g}(\omega) = \frac{1}{\omega - \Gamma} \tag{1.18}$$

with $\Gamma_{rs} = \delta_{rs}\omega_r$ and $\omega_r = \begin{pmatrix} \omega^{(e)} & \omega^{(h)} \end{pmatrix}$
gives us the

LEHMAN REPRESANTATION OF THE ZERO-TEMPERATURE GREEN FUNCTION [22]

$$\mathbf{G}(\omega) = \mathbf{Q}\mathbf{g}(\omega)\mathbf{Q}* \tag{1.19}$$

1.1.3 The many-body real-time Green function

Following [27], the starting point to derive an expression for the retarded many-body real-time Green function is chosen to be the n-body real-time time-ordered Green function

$$G^{(n)}(\alpha_1 t_1, ..., \alpha_n t_n | \alpha'_1 t'_1, ..., \alpha'_n t'_n) = (-i)^n \left\langle T \left[c^{(H)}_{\alpha_1}(t_1) ... c^{(H)}_{\alpha_n}(t_n) c^{(H)\dagger}_{\alpha'_n}(t'_n) ... c^{(H)\dagger}_{\alpha'_1}(t'_1) \right] \right\rangle . \tag{1.20}$$

The creation and annihilation operators $c^{(H)}_{\alpha_i}(t)$ and $c^{(H)\dagger}_{\alpha_i}(t)$ are represented in the Heisenberg picture and α_i denotes a state, including spin and site. The T describes a time ordered product and the brackets a thermal average. To treat the Green function further, a thermodynamic ensemble has to be chosen. As in the canonical ensemble, the number of particles N in a system is fixed, it is no practical to be used. A more suitable solution is found in the grand canonical ensemble,

as it allows the exchange of particles of the system with the environment. When talking about the grand canonical ensemble it is necesarry to introduce the **chemical potential** μ, which leads to a transformation of the Hamilton-Operator

$$H \to H - \mu N \tag{1.21}$$

To simplify any further calculations the Hamiltonian will still be written as H but has to be understood as $H - \mu N$. The definition of an expecation value of an operator is

$$\langle O \rangle = \frac{tr\left(Oe^{-\beta H}\right))}{tr\left(e^{-\beta H}\right)} \tag{1.22}$$

applying that onto 1.20 gives

$$G^{(n)}(\alpha_1 t_1, ..., \alpha_n t_n | \alpha'_1 t'_1, ..., \alpha'_n t'_n) = \frac{(-i)^n}{Z} Tr\left(e^{-\beta H} T\left[c^{(H)}_{\alpha_1}(t_1)...c^{(H)}_{\alpha_n}(t_n) c^{(H)^\dagger}_{\alpha'_n}(t'_n)...c^{(H)^\dagger}_{\alpha'_1}(t'_1)\right]\right) \tag{1.23}$$

with $Z = Tr(e^{-\beta H})$ being the grand canonical partition function. Following [27], now the creation and annihilation operators will be replaced with the corresponding field operators $\Psi(x,t)$

$$\Psi(x,t) = e^{iHt}\Psi(x)e^{-iHt} \widehat{=} e^{iHt} c_{\alpha_i} e^{-iHt} \tag{1.24}$$

yields the result for the annihilation operator c_{alpha_i}. The same transformation holds also for the creation operator $c^\dagger_{\alpha_i}$. With the represantation of the operators in second quantization and the grand canonical ensemble, the expression for the many-body Green function can now be written as

$$G^{(n)}(x_1 t_1, ..., x_n t_n | x'_1 t'_1, ..., x'_n t'_n) = (-i)^n \left\langle T\left[\Psi(x_1,t_1)...\Psi(x_n,t_n)\Psi^\dagger(x'_n,t'_n)...\Psi^\dagger(x'_1,t'_1)\right]\right\rangle, \tag{1.25}$$

where the angular brackets denote the expecation value again. Having the creation and annihilation operators written in second quantization also solves the problem of both, imaginary and real time appearing in 1.23. Imaginary times appeared in the exponential functions of the creation and annihilation operators. If one takes the ground state expecation value, the so-called **zero-temperature Green function** can be obtained from 1.25:

$$G^{(n)}(x_1 t_1, ..., x_n t_n | x'_1 t'_1, ..., x'_n t'_n) = (-i)^n \left\langle \psi_o \left| T\left[\Psi(x_1,t_1)...\Psi(x_n,t_n)\Psi^\dagger(x'_n,t'_n)...\Psi^\dagger(x'_1,t'_1)\right] \right| \psi_0 \right\rangle \tag{1.26}$$

1.1.4 The single-particle zero-temperature Green function

Many physical properties can be described conveniently by **single-particle Green functions** which shall now be introduced. First a more compact notation is brought in, where space-time points $\{x_n t_n\}$ are replaced by n, so 1.25 becomes

$$G^{(n)}(1,...,n|1',...,n') = (-i)^n \left\langle \psi_o \left| T\left[\Psi(1)...\Psi(n)\Psi^\dagger(n')...\Psi^\dagger(1')\right] \right| \psi_0 \right\rangle \tag{1.27}$$

and in case of a single particle (n=1)

$$G(1|1') = (-i)\left\langle T\left[\Psi(1)\Psi^\dagger(1')\right]\right\rangle, \tag{1.28}$$

where the superscript $^{(n=1)}$ has been, and will be in the following definitions, neglected. With only two wave functions left in the single-particle Green function there are only two time-ordering possiblities left as well: $t_1 > t_{1'}$ and $t_1 < t_{1'}$. These two time orders can be distinguished by the following

$$G(1|1') = \Theta(t_1 - t_{1'})G^>(1|1') + \Theta(t_{1'} - t_1)G^<(1|1'), \tag{1.29}$$

introducing the

GREATER GREEN FUNCTION

$$G^>(1|1') = -i\left\langle \Psi(1)\Psi^\dagger(1')\right\rangle \tag{1.30}$$

and the

LESSER GREEN FUNCTION

$$G^>(1|1') = -i\zeta\left\langle \Psi^\dagger(1')\Psi(1)\right\rangle, \tag{1.31}$$

which has been defined for Bosons ($\zeta = 1$) and Fermions ($\zeta = -1$).
Combining the greater and the lesser Green function leads to the already known

ADVANCED GREEN FUNCTION

$$G^{av}(1,1') = (G^<(1|1') - G^>(1|1'))\Theta(t_{1'} - t_1) \tag{1.32}$$

$$= i\left\langle \left[\Psi(1)\Psi^\dagger(1')\right]_{-\zeta}\right\rangle \Theta(t_{1'} - t_1) \tag{1.33}$$

and the

RETARDED GREEN FUNCTION

$$G^{ret}(1,1') = (G^{>}(1|1') - G^{<}(1|1'))\Theta(t_1 - t_{1'}) \quad (1.34)$$

$$= -i\left\langle \left[\Psi(1)\Psi^{\dagger}(1')\right]_{-\zeta}\right\rangle \Theta(t_1 - t_{1'}) \quad (1.35)$$

which has also been defined for bosons, using the commutator $[A,B]_+ \equiv [A,B]$ as well as fermions, using the anti-commutator $[A,B]_- \equiv \{A,B\}$. Furthermore it has to be noted that the retarded Green function is only non-zero for $t_1 > t_{1'}$ and the advanced Green function is only non-zero for the opposite case $t_{1'} > t_1$.

1.2 Cluster perturbation theory

CPT is a method to solve quantum multi-body problems by dividing larger, or even infintely large systems into smaller clusters, which can be solved exactly e.g. by Exact Diagonalization methods (ED). These solved clusters can then gradually be connected to or embedded in the full lattice. As the CPT approach naturally only considers short-range correlations it can only be seen as **exact** in the non-interacting limit. To represent best the effect of the surrounding infinite (or full) lattice, additional fields, or bath degrees of freedom are added to the cluster [38]. Following [38] the derivation of the central equations used in CPT is sketched in this chapter. The underlying model is the one-band Hubbard model on a lattice γ. The sites shall be labelled by position vectors $(\mathbf{r}, \mathbf{r'}, ...)$. The destruction operator for an electon on site $\mathbf{r}$ with spin σ is $c_{\mathbf{r}\sigma}$ and the number operator is $n_{\mathbf{r}\sigma}$. The Hamiltonian for the lattice then reads as

$$H = \sum_{\mathbf{r},\mathbf{r'},\sigma} t_{\mathbf{r},\mathbf{r'}} c^{\dagger}_{\mathbf{r}\sigma} c_{\mathbf{r'}\sigma} + U \sum_{\mathbf{r}} n_{\mathbf{r}\uparrow} n_{\mathbf{r}\downarrow} - \mu \sum_{\mathbf{r}} n_{\mathbf{r}} \quad (1.36)$$

with $t_{\mathbf{r},\mathbf{r'}}$ the hopping matrix, μ the chemical potential and U the one-site Coulomb repulsion.

1.2.1 Cluster decomposition

Dividing the full lattice γ into identical clusters with L sites inside, corresponds to introducing a superlattice Γ. The sites of the superlattice Γ form a subset of the lattice γ and are labelled by vectors $\mathbf{r}^{\Gamma}$. The sites of the cluster will be labelled by capital vectors $\mathbf{R}$. Now every site $\mathbf{r}$ of the original lattice γ can be reached by a linear combination $\mathbf{r} = \mathbf{r}^{\Gamma} + \mathbf{R}$.

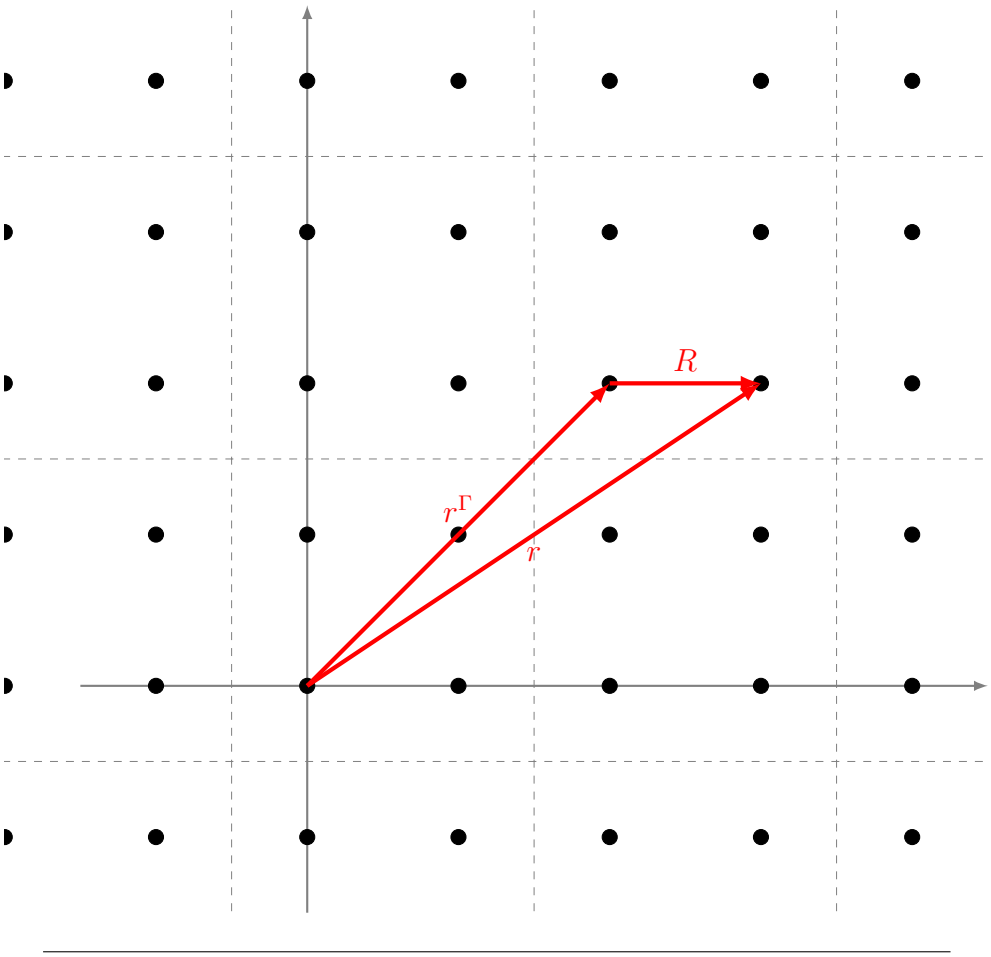

FIGURE 1.1: Cluster decomposition of a 2D lattice into 4-site clusters

With this cluster tiling the Hamiltonian now is written as

$$H = H' + V, \tag{1.37}$$

with H' the cluster Hamiltonian, with hoppings strictly inside a certain cluster and V the matrix of inter-cluster hopping, i.e. the hopping from one cluster to another. Taking another look at $\mathbf{V}$ in second quantization gives

$$\mathbf{V} = \sum_{r^\Gamma, r^{\Gamma'}} \sum_{a,b} T_{a,b}^{r^\Gamma, r^{\Gamma'}} c^\dagger_{r^\Gamma, a} c_{r^{\Gamma'}, b}. \tag{1.38}$$

The hopping matrix $T_{a,b}^{r^\Gamma, r^{\Gamma'}}$ only has non-zero entries for inter-cluster hoppings. According to the notation used it describes the hopping between sites a and b of two different clusters r^Γ and $r^{\Gamma'}$. Using strong-coupling perturbation theory [37] [39] it can be shown that the lowest order result for the lattice Green function then is

THE CENTRAL EQUATION FOR CPT

$$\mathbf{G}^{-1}(\omega) = \mathbf{G}_0^{-1}(\omega) - \mathbf{T}, \tag{1.39}$$

with $\mathbf{G}_0(\omega)$ the exact Green function of the cluster and $\mathbf{T}$ the inter-cluster hopping matrix. Looking at the matrices $\mathbf{G}$, $\mathbf{G}_0$ and $\mathbf{T}$ it is important to point out that they are in the space $E = \gamma \otimes B$, with γ the lattice and B the band and spin states. B will be ignored, due to spin-symmetry of the systems in this thesis. The exact Green function of the cluster $\mathbf{G}_0$ is identical for all clusters.
The fully interacting Green function of the isolated cluster can also be written in terms of a self-energy Σ [8]:

$$\mathbf{G}_0^{-1}(\omega) = (\mathbf{G}_0^0)^{-1}(\omega) - \Sigma^0(\omega), \tag{1.40}$$

with $(\mathbf{G}_0^0)^{-1}(\omega)$ the Green function of the non interacting isolated cluster, i.e. $U = 0$ and $\Sigma^0(\omega)$ the self-energy of the cluster. The Green function of the non interacting isolated cluster further is

$$(\mathbf{G}_0^0)^{-1}(\omega) = \omega - \mathbf{T}^0, \tag{1.41}$$

which leads to

$$\mathbf{G}_0^{-1}(\omega) = \omega - \mathbf{T}^0 - \Sigma^0(\omega). \tag{1.42}$$

The same thought about the non-interacting Green function of the full latice gives

$$(\mathbf{G}^0)^{-1}(\omega) = \omega - \mathbf{T}^{tot} = \omega - (\mathbf{T} + \mathbf{T}^0), \tag{1.43}$$

with $\mathbf{T}$ the hopping matrix of the inter-cluster hoppings and $\mathbf{T}^0$ the hopping matrix of intra-cluster hoppings.
Plugging those equations into 1.40 yields

$$\mathbf{G}_0^{-1}(\omega) = (\mathbf{G}^0)^{-1}(\omega) + \mathbf{T} - \Sigma^0(\omega), \tag{1.44}$$

giving another Dyson equation for the whole system

$$\mathbf{G}^{-1}(\omega) = (\mathbf{G}^0)^{-1}(\omega) - \Sigma(\omega), \tag{1.45}$$

with $\Sigma(\omega)$ the self-energy of the whole system, yields another form of

THE CENTRAL EQUATION FOR CPT IN TERMS OF SELF-ENERGY

$$\mathbf{G}^{-1}(\omega) = \mathbf{G}_0^{-1}(\omega) - \mathbf{T} - (\Sigma(\omega) - \Sigma^0(\omega)), \tag{1.46}$$

Characteristics of CPT CPT is derived with the help of strong-coupling perturbation theory. It is therefore an approximation and needs not to be exact. However, there are some limiting cases for which CPT gives exact results:

1. U $\to$ 0: The self-energy disappears in this case and CPT gives exact results.
2. Strong-coupling limit $\frac{t_{rr'}}{U} \to 0$: In this case $t_{rr'}$ describes the hopping between neighboring atoms. Considering the case $t_{rr'} = 0$ gives the simple atomic problem, it is obvious that CPT gives the exact results in this case.
3. Infinite cluster size: The whole lattice would be solved by ED. Depending on the system's size such an approach is possible or not.

Furthermore, CPT cannot describe broken-symmetry cases. However, this can be achieved by using VCA which will be discussed later in the present work.
Finally, CPT gives an approximate lattice Green function for arbitrary wave vectors which makes it a usefull tool when comparing with ARPES data. While CPT does not have self-consistency, that is for example given in DMFT approaches, it does allow for the best momentum resolution at fixed computing resources.

1.3 Keldysh formalism

When doing transport calculations the Keldysh nonequilibrium Green function formalism (KNEGF) is an important tool. To get a full grasp one could read the book by Haug and Jauho [15].
The following considerations are based mainly on the lecture notes of Jauho [17] as well as [34]. As it is not sufficient anymore to treat the Green functions in the equilibrium case, it is therefore necessary to expand the equilibrium Green function formalism further into the so-called **Keldysh space**. The KNEGF is often also referred to as Contour ordered Green function technique and was named Keldysh formalism after the work of Keldysh in 1964 [18].
The starting point shall be the zero-temperature single-particle Green function 1.28

$$G(x,t;x',t') = \frac{-i}{\hbar}\frac{\langle\psi_0|\, T\{\psi_H(x,t)\psi_H^\dagger(x',t')\}\,|\psi_0\rangle}{\langle\psi_0|\psi_0\rangle}, \tag{1.47}$$

where the space-index x will be surpressed, as well as $\hbar = 1$

$$G(t|t') = -i\frac{\langle\psi_0|\, T\{\psi(t)\psi^\dagger(t')\}\, |\psi_0\rangle}{\langle\psi_0|\psi_0\rangle}, \tag{1.48}$$

The Hamiltonian of the considered system can be written as

$$H = H_0 + H_1(t) \tag{1.49}$$

where H_0 describes the non-interacting system and $H_1(t)$ contains all the many-body aspects of the problem. It is convenient to set

$$H_1(t) = e^{-\eta|t|}V(t) \tag{1.50}$$

with η being a positive infinitesimal, and $V(t)$ describing the perturbation of the system.
Taking a look at what happens when approaching infinite negative times gives

$$\lim_{t\to-\infty} H_1(t) = 0 \to \lim_{t\to-\infty} H(t) = H_0, \tag{1.51}$$

which is convenient because the exact ground state of a system $|\psi_0\rangle$ now corresponds to the ground state of the non-interacting system φ_0 in the limit $t \to -\infty$. Now the S-matrix is introduced, that changes the wave function from $\psi(t')$ to $\psi(t)$:

$$\psi(t) = S(t,t')\psi(t'). \tag{1.52}$$

So S can be written in terms of the unitary operator U:

$$S(t,t') = U(t)U^\dagger(t'). \tag{1.53}$$

It is important to point out that the S-matrix obeys the following group property

$$S(t,t') = S(t,t'')S(t'',t'). \tag{1.54}$$

As the ground state is one of the quantities one wants to calculate with the Green function formalism, the definition 1.47 yields the problem of having the ground state within the definition itself. Therefore it is necessary to express the exact ground state $|\psi_0\rangle$ in terms of known quantities, for example the non-interacting ground state $|\varphi_0\rangle$. The Gell-Mann and Low theorem gives [8]:

$$|\psi_0\rangle = S(0,-\infty)\,|\varphi_0\rangle\,^{1} \tag{1.55}$$

Using the expression for the groundstate 1.55, the identity $(S(0,-\infty)\,|\varphi_0\rangle)^* \equiv \langle\varphi_0|\, S(-\infty,0)$ and applying both onto the zero-temperature Green function 1.48 yields

$$G(t|t') = -i\frac{\langle\varphi_0|\, S(-\infty,0)T\left[\psi(t)\psi^\dagger(t')\right] S(0,-\infty\,|\varphi_0\rangle}{\langle\varphi_0|\, S(-\infty,0)S(0,-\infty)\,|\varphi_0\rangle} \tag{1.56}$$

[1] This equation is justified significantly by 1.51

The operators as well as the wave functions unto this point were depicted in the Heisenberg picture. Now they shall be represented in the interaction picture with respect to H_0, giving

$$|\Psi^{I,H_0}\rangle = S(t,-\infty)\,|\Psi\rangle = S(t,-\infty)\,|\varphi_0\rangle \tag{1.57}$$

$$O^{(H)}(t) = S(-\infty,t)O^{I,H_0}(t)S(t,-\infty) \tag{1.58}$$

Applying these transformations onto eq. 1.56 and taking advantage of the group properties of the S-Matrix gives

$$G(t|t') = -i\frac{\langle\varphi_0|\, S(-\infty,t)T\left[S(t,-\infty)\psi(t)\psi^\dagger(t')\right]|\varphi_0\rangle}{\langle\varphi_0|\,|\varphi_0\rangle} \tag{1.59}$$

Note: $S(t,-\infty)$ was pulled inside the argument of the time-ordering operator T. $S(-\infty,t)$ cannot be pulled inside, because it does not feature the required time-order due to $t > -\infty$. It is possible to solve this problem in the equilibrium case, by introducing the ground state in the distant future, however since this chapter focuses on the non-equilibrium, the derivation is left out.

1.3.1 Non-equilibrium case

In the non-equilibrium case a new technique to solve the problem has to be introduced: The **Contour Ordered Green function technique**. This requires the introduction of the so-called Keldysh contour. To do so eq. 1.59 has to be changed a little by inserting an identity $\mathbb{1} = S(t,\infty)S(\infty,t)$ in front of T.

$$G(t|t') = -i\frac{\langle\varphi_0|\, S(-\infty,\infty)T\left[S(\infty,-\infty)\psi(t)\psi^\dagger(t')\right]|\varphi_0\rangle}{\langle\varphi_0|\,|\varphi_0\rangle} \tag{1.60}$$

Now to handle the $S(-\infty,\infty)$ term a closed path, the Keldysh contour is introduced. This corresponds to an evolution of the system from $t \to \infty$ to $t \to \infty$ in forward time direction and back again, along different contour branches. This situation is depicted in 1.2

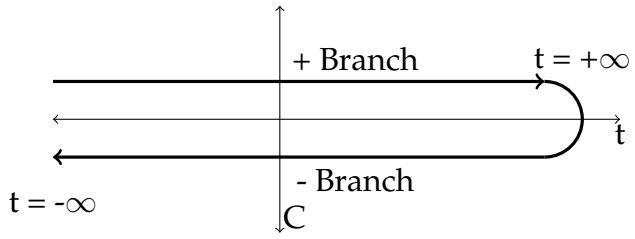

FIGURE 1.2: The Keldysh Contour

This goes hand in hand with the necessity of extending the time-ordering operator T to the contour-ordering operator T_C according to

$$T_C[O_A(t_1,C_1)O_B(t_2,C_2)] = \begin{cases} O_A(t_1,C_1)O_B(t_2,C_2), \text{for} \{t_1,C_1\} > \{t_2,C_2\} \\ O_B(t_2,C_2)O_A(t_1,C_1), \text{for} \{t_2,C_2\} > \{t_1,C_1\} \end{cases} \tag{1.61}$$

times on the + branch appear earlier in the sense of the Keldysh contour than times on the - branch. This allows to order all operators inside the argument of the contour-ordering operator T_C along a particular contour, which allows for $S(-\infty, \infty)$ to be pulled inside said operator:

$$G(t_1 C_1 | t_2 C_2) = -i \frac{\langle \varphi_0 | \, T_C \left[S(-\infty, -; \infty) S(\infty; -\infty, +) \psi(t_1, C_1) \psi^\dagger(t_2 C_2 \right] | \varphi_0 \rangle}{\langle \varphi_0 | \, | \varphi_0 \rangle} \tag{1.62}$$

The contour-ordered Green function now contains four different functions:

$$G(t_1|t_2) = \begin{pmatrix} G^C(t_1|t_2) & G^<(t_1|t_2) \\ G^>(t_1|t_2) & G^{\tilde{C}}(t_1|t_2) \end{pmatrix} \tag{1.63}$$

with the introduction of four Green functions:

THE TIME-ORDERED GREEN FUNCTION

$$G^C(1|2) = -i \left\langle T \left[\psi(1) \psi^\dagger(2) \right] \right\rangle \tag{1.64}$$

THE GREATER GREEN FUNCTION

$$G^>(1|2) = -i \left\langle \psi(1) \psi^\dagger(2) \right\rangle \tag{1.65}$$

THE LESSER GREEN FUNCTION

$$G^<(1|2) = -i\zeta \left\langle \psi^\dagger(1) \psi(2) \right\rangle \tag{1.66}$$

THE ANTITIME-ORDERED GREEN FUNCTION

$$G^C(1|2) = -i\left\langle \tilde{T}\left[\psi(1)\psi^\dagger(2)\right]\right\rangle \tag{1.67}$$

Remark: The quantum number n that combines time-, space-, spin-, ... coordinates has been used again. The angle brackets, again, denote an expecation value concerning the ground state $|\varphi_0\rangle$ of the non-interacting system. $\zeta = -1$ for Fermions and $\zeta = 1$ for Bosons.
The retarded/advanced Green function can be described in terms of the Lesser/Greater Green function:

$$G^r(1|2) = (G^>(1|2) - G^<(1|2))\Theta(t_1 - t_2) \tag{1.68}$$
$$G^a(1|2) = (G^<(1|2) - G^>(1|2))\Theta(t_2 - t_1). \tag{1.69}$$

The four components are not linearly independent

$$G^C(1|2) + G^{\tilde{C}}(1|2) = G^<(1|2) + G^>(1|2) := G^K(1|2) \tag{1.70}$$

introducing the Keldysh Green function G^K. Due to this linear dependence it is possible to perform a rotation in Keldysh space:

$$G(1|2) = \begin{pmatrix} G^C(1|2) & G^<(1|2) \\ G^>(1|2) & G^{\tilde{C}}(1|2) \end{pmatrix} \rightarrow \begin{pmatrix} G^r(1|2) & G^K(1|2) \\ 0 & G^a(1|2) \end{pmatrix} := \tilde{G}(1|2) \tag{1.71}$$

1.3.2 Electrical current densitiy for interacting systems

With the Keldysh formalism it is now possible to calculate the steady-state electrical current density $j_{nn'}$ between neighboring sites n and n'. Steady-state means the physical situation, where the initial correlations can be neglected due to the interactions.
In this work all the electrical field driven currents are due to a linear increasing potential from left to right. The current density between sites n and n' is given by

$$j_{nn'} = i\frac{e}{\hbar}t_{nn'}\left\langle c_n^\dagger c_{n'} - c_{n'}^\dagger c_n\right\rangle \tag{1.72}$$

with e the electronic charge and $\hbar$ the reduced Planck constant, that will be both set to 1 in the following derivations.
Using the commutator relation for fermions $\left[c_i, c_j^\dagger\right] = \delta_{ij}$ on eq. 1.72 gives

$$\begin{aligned} j_{nn'} &= it_{nn'} \left\langle c_n^\dagger c_{n'} - c_{n'}^\dagger c_n \right\rangle \\ &= i\frac{t_{nn'}}{2} \left\langle \left(c_n^\dagger c_{n'} + c_n^\dagger c_{n'}\right) - \left(c_{n'}^\dagger c_n + c_{n'}^\dagger c_n\right) \right\rangle \\ &= i\frac{t_{nn'}}{2} \left\langle \left(c_n^\dagger c_{n'} + c_{n'}^\dagger c_n + \delta_{nn'}\right) - \left(c_{n'}^\dagger c_n + c_n^\dagger c_{n'} + \delta_{n'n}\right) \right\rangle \\ &= \frac{t_{nn'}}{2} \left(i \left\langle c_n^\dagger c_{n'} \right\rangle + i \left\langle c_{n'} c_n^\dagger \right\rangle - i \left\langle c_{n'}^\dagger c_n \right\rangle - i \left\langle c_n c_{n'}^\dagger \right\rangle \right) \end{aligned} \tag{1.73}$$

using the definitions of the Greater and Lesser Green function (eq. 1.30 and eq. 1.31) gives

$$\begin{aligned} j_{nn'} &= \frac{t_{nn'}}{2} \left(G^<_{nn'} - G^>_{n'n} - G^<_{n'n} + G^>_{nn'} \right) \\ &= \frac{t_{nn'}}{2} \left(G^K_{nn'} - G^K_{n'n} \right) \end{aligned} \tag{1.74}$$

where eq. 1.70 was used.
Eq. 1.74 simplifies with the relationship $G^K = -(G^K)^\dagger$ further to

$$\begin{aligned} j_{nn'} &= \frac{t_{nn'}}{2} \left[G^K_{nn'} + (G^K_{nn'})^\dagger \right] \\ &= t_{nn'} \Re\{G^K_{nn'}(t,t)\} \end{aligned} \tag{1.75}$$

with the introduction of the explicit time-dependency. Fourier transforming this equation with respect to the time t into frequency space finally yields

$$j_{nn'} = \frac{t_{nn'}}{2} \int_{-\infty}^{\infty} d\omega \Re\{G^K_{nn'}(\omega)\}. \tag{1.76}$$

Chapter 2

Electronic transport in a one-dimensional tight-binding Hubbard chain

2.1 Introduction

The behaviour of solids, driven out of equilibrium, by external fields has been one of the major topics of condensed matter physics for the past decades [3]. Its understanding is crucial to the development of nanotechnological applications like resistive transitions. [23] The theoretical approach contains developing and improving new and old numerical methods and approximations to treat and describe models for said systems. This work builds up to treating a relatively simple model with the variational cluster approximation method.
In this chapter we look at the electronic transport in a finite one-dimensional chain, by using cluster perturbation theory (CPT). The chain underlies a homogenous electric field to create a current flowing, so the system will be out of equilibrium and corresponding methods have to be used. In detail, the keywords are cluster perturbation theory (CPT) and Keldysh non-equilibrium Green function formalism (KNEGF). In the later chapters of this thesis the variational cluster approximation (VCA) will be introduced to furthermore improve the results in the interacting case.
The model for these calculations is a finite one-dimensional tight-binding Hubbard chain which will be explained in the next section. It has to be stated that calculations on an infinite one-dimensional tight-binding Hubbard chain have been done previously on the institute of theoretical physics at the TU Graz [29]. These results were taken as a comparison for the calculations done on the finite model.
Felix Bloch [4] and Clarence Zener [43] predicted (in 1929 by Felix Bloch and 1934 by Clarence Zener) that electrons, captured in periodic potentials in the presence of a homogenous electric field, will be forced to oscillate around a central position, rather than being moved uniformly in the direction of the electric field. These so-called Bloch oscillations were finally observed nearly 70 years later in semiconductor superlattices by optical investigations [7]. However, these Bloch oscillations are very hard to observe in solids. This derives from the scattering of electrons with acoustic phonons and impurities in real crystal structures. As in

the models treated in this work, phonon interations as well as impurities are completely neglected due to simplicity, dissipation mechanisms of some form have to be implemented to the models.
The suppression of Bloch oscillations due to dissipation mechanisms, like periodical driven systems [41] became an important topic when dealing with non-equilibrium transport calculations in strongly correlated systems.
In this work the dissipation mechanism used is to couple fermionic bath chains to the physical sites of a tight-binding chain which is in fact a rather common method [13] [2]. It has been stated that this model is a rather simple one [13], but although it is not as sophisticated as other approaches it provides a good minimal setup for studying non-equilibrium transport calculations.

2.2 Model and Methods

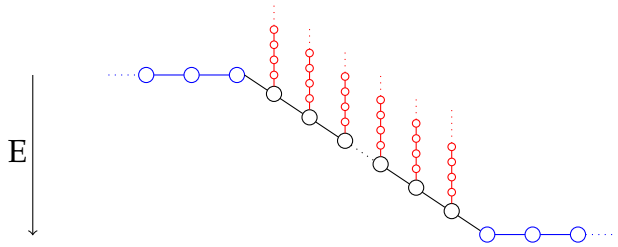

FIGURE 2.1: A finite Hubbard chain with correlated electrons in a homogenous E field attached to leads

As depicted in 2.1 the system can be partioned into several segments. The blue parts are two semi-infinite tight-binding chains with hopping parameters t_{ll}. These semi-infinite chains are coupled to the central region (the black part) with hopping parameter t_{lc} for the left and t_{cl} for the right lead. Each physical site in the central region is coupled to a semi-infinte tight-binding chain (red part) with a hopping parameter t_{cb}. The hopping in those bath chains is t_{bb}. Finally the hopping parameter in the central region is t_{cc}. The leads as well as the bath chains do not suffer from a correlation i.e. the Hubbard interaction $U = 0$ at all times. Electrons in the central region are correlated with a hubbard interaction U that can be nonzero.
The Hamiltonian of the system can therefore also be separated into the following parts:

$$H_{cc} = -t_{cc} \sum_{<i,j>}^{N_{cc}} (\hat{c}_i^\dagger \hat{c}_j + h.c.) + U \sum_{i,j} \hat{n}_i \hat{n}_j \tag{2.1}$$

$$H_{bb} = -t_{bb} \sum_{<i,j>}^{\infty} (\hat{c}_i^\dagger \hat{c}_j + h.c.) \tag{2.2}$$

$$H_{ll} = -t_{ll} \sum_{<i,j>}^{\infty} (\hat{c}_i^\dagger \hat{c}_j + h.c.) \tag{2.3}$$

$$H_{cl} = -t_{cl}(\hat{c}^{\dagger}_{c_{N_{cc}}}\hat{c}_{l_1} + h.c.) \tag{2.4}$$

$$H_{lc} = -t_{cl}(\hat{c}^{\dagger}_{c_{l_1}\hat{c}_{N_{cc}}} + h.c.) \tag{2.5}$$

2.3 1-site cluster

To solve the system, the solution for the cluster has to be found first. The cluster consists of a few of the physical bath sites (in this case a few actually means just one), which then is coupled via CPT to the corresponding heat baths. The resulting Green function, with the baths already coupled to the central cluster shall be denoted by g^{cc} as oposed to the isolated cluster g_0^{cc}. The Dyson equation then yields

$$g^{cc} = g_0^{cc} + g_0^{cc}t^{cb}g^{bc}$$
$$g^{bc} = g_0^{bb}t^{bc}g^{cc}$$

The index b includes a sum over all connected bath sites. Following the notation already stated, g_0^{bb} is the Green function of the isolated bath chains at the first site of the half infinte chain which is connected to the central cluster. This makes g_0^{bb} a diagonal matrix $g_0^{bb} = \text{diag}\{g_j^{(b)}\}$, where $g_j^{(b)}$ is the local GF at the first site of the isolated bath chain which is attached to the physical site with index j.
So

CLUSTER GF ALREADY COUPLED TO BATH

$$g^{cc} = g_0^{cc} + g_0^{cc}\Gamma g^{cc}$$
$$\Gamma_{ij}(\omega) = \delta_{ij}\left(t^{cb}\right)^2 g_j^b(\omega)$$

To connect the clusters along the chain direction the cluster Green function has to be shifted by Δx_n,

$$g_n^{cc}(\omega) = g^{cc}(\omega - E\Delta x_n)$$

The retarded and advanced part of the cluster Green function follows directly from

RETARDED/ADVANCED PART OF CLUSTER GF COUPLED TO BATH

$$\left(g^{cc.a}\right)^{-1} = \left(g_0^{cc.a}\right)^{-1} - \Gamma^a \ . \tag{2.6}$$

To obtain the Keldysh component, the Kadanoff-Baym [3] relation is used

$$g^{cc.K} = g^{cc.r}\left\{\left(g_0^{cc.r}\right)^{-1} g_0^{cc.K}\left(g_0^{cc.a}\right)^{-1} + \Gamma^K\right\} g^{cc.a} \ . \tag{2.7}$$

Since g_0 is an equilibrium Green function

$$g_0^{cc.K}(\omega) = \Big(2f(\omega|\mu) - 1\Big)\left[g_0^{cc.a}(\omega) - g_0^{cc.r}(\omega)\right]$$

The first part in eq. 2.7 yields

$$\begin{aligned}
&\left(g_0^{cc.r}\right)^{-1}\left\{\left(2f(\omega) - 1\right)\ \left[g_0^{cc.a} - g_0^{cc.r}\right]\right\}\left(g_0^{cc.a}\right)^{-1} \\
&\qquad = \left(2f(\omega) - 1\right)\left\{\left(g_0^{cc.r}\right)^{-1} - \left(g_0^{cc.a}\right)^{-1}\right\} \\
&\qquad = 2i0^+\ \left(2f(\omega) - 1\right)
\end{aligned}$$

In the limit $0^+ \to 0$ the first part vanishes, so

$$g^{cc.K} = g^{cc.r}\Gamma^K g^{cc.a} \ . \tag{2.8}$$

Now eq. 2.7 is applied to the bath Green function

$$\begin{aligned}
\Gamma^K(\omega) &= \mathrm{diag}\left(t^{cb}\right)^2 \left\{g_j^{b.K}(\omega)\right\} \\
g_j^{b.K}(\omega) &= 2i\Big(f(\omega|\mu_j) - 1\Big)\Im\Big(g_j^{b.a}(\omega)\Big)
\end{aligned}$$

The chemical potential is defined as

$$\mu_j = -Ej + \Delta\mu_j$$

so

$$g_j^{b.K}(\omega) = 2i\Big(f(\omega - Ej|\Delta\mu_j) - 1\Big)\Im\Big(g_0^{b.a}(\omega - Ej)\Big) = g_0^{b.K}(\omega - Ej|\Delta\mu_j)$$

So for the

KELDYSH PART OF CLUSTER GF COUPLED TO BATH

$$g^{cc.K} = g^{cc.r}\Gamma^K g^{cc.a} \tag{2.9}$$

$$\Gamma^K(\omega) = \left(t^{cb}\right)^2 \text{diag}\Big\{g_0^{b.K}(\omega - \mu_j|\Delta\mu_j)\Big\} \tag{2.10}$$

$$g_0^{b.K}(\omega|\Delta\mu_j) = 2i\Big(f(\omega|\Delta\mu_j) - 1\Big)\Im\Big(g_0^{b.a}(\omega)\Big) \tag{2.11}$$

It has to be pointed out that the translational invariance in the form $g_j(\omega) = g(\omega - Ej)$ is violated for $\Delta\mu_j \neq 0$. $\Delta\mu_j$ was introduced to suppress particle flow into the heat baths.
The chemical potential in this work was chosen in a way to describe the Hubbard model at half filling. In detail this means that the total number of fermions in the system is exactly the number of lattice sites and the chemical potential $\mu = \frac{U}{2}$.
As the Green functions of the bath chains are equivalent to each other (apart from an energy-shift), they only have to be calculated once. There are two different approaches for the Green function of one of those bath chains used in this work.

SEMI-INFINTE TIGHT-BINDING CHAIN [6]

$$g_0^{b.a}(\omega) = \frac{\omega}{2t_{bb}^2} \pm \frac{1}{t_{bb}}\sqrt{(\frac{\omega}{2t_{bb}})^2 - 1} \tag{2.12}$$

WIDE-BAND LIMIT

$$g_0^{b.a}(\omega) = i\Gamma \tag{2.13}$$

t_{bb} denotes the next-neighbour hopping inside the bath chain and $\Gamma = \frac{t_{bc}^2}{t_{bb}}$ is the so-called damping parameter, occuring in the wide band limit, with t_{bc} the coupling strength of the bath chain to the central region. As the name wide-band limit suggests this approach is suitable for high hopping parameters, which gives a wide bandwidth. Further analysis of the range of application of the wide-band limit will be discussed later on in this chapter.

2.3.1 Left and right half-infinite chain

After having coupled the isolated central cluster to its heat bath, the chain can be built up by coupling the Green functions via CPT. The coupling can be performed from the left as well as the right. In fact one has to build both chains first.

Building the lead Green functions

When constructing the Green function of the leads, one has to keep in mind how to treat the chemical potential when shifting the Green function in energy space.

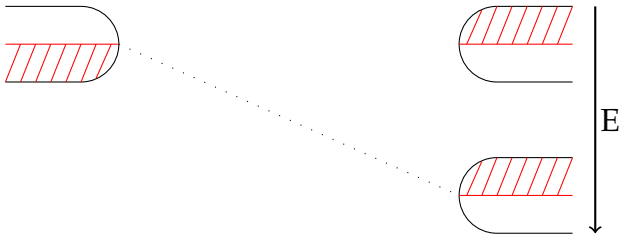

FIGURE 2.2: The position of the chemical potential in the energy space is denoted by the red line. The band is half-filled in that case, meaning the chemical potential is fixed relative to the band. When the whole lead is shifted in energy, the band stays half filled.

As shown in the picture above, the band of the leads stays half-filled for all values of E. So one expects a non-zero current, when the half-filled parts of the bands overlap.

Left to right

Starting with the left lead and iteratively adding clusters gives the left half-infinite chain. Let $G^n := G^{(n,n)}$ be the cluster GF of a chain that consists of the left lead plus the first n clusters, so G^0 is the local GF of the contact point of the left lead. For the first step

$$G^{11} = g^{11} + g^{11}T^{10}G^{01}$$
$$G^{01} = g^{00}T^{01}G^{11}$$

Iteratively coupling via the GFs via Dyson equation gives

$$\begin{aligned} G^{nn} &= g^{nn} + g^{nn} t_{n,n-1} G^{n-1,n} \\ G^{n-1,n} &= g^{n-1,n-1} t_{n-1,n} G^{nn} \\ G^{nn} &= g^{nn} + g^{nn} t_{n,n-1} g^{n-1,n-1} t_{n-1,n} G^{nn} \ . \end{aligned}$$

The notation shall now be simplified by abbreviating G^{nn} with G^n and g^{nn} with g^n. Furthermore, the fact is used, that $g^{n-1,n-1} = G^{n-1,n-1}$, so

$$\begin{aligned} G^n &= g^n + g^n \Big(t_{n,n-1} G^{n-1} t_{n-1,n} \Big) G^n \\ G^n &= g^n + g^n \big(t^2_{n-\frac{1}{2}} G^{n-1} \big) G^n \\ t_{n-\frac{1}{2}} &:= t_{n,n-1} = t_{n-1,n} \end{aligned}$$

Looking closely at $t_{n-\frac{1}{2}}$, one finds that for $n = 1$ $t_{\frac{1}{2}} := t_{1,0} = t_{cl}$ which describes the hopping from the lead to the central region. For $n = 2, ..., L$, $t_{n-\frac{1}{2}} := t_{n,n-1} = t_{cc}$, one finds the hopping inside the central region. Finally for $n = N_{cc} + 1$ the hopping is $t_{N_{cc}+\frac{1}{2}} := t_{N_{cc}+1,N_{cc}} = t_{cl}$, which describes the hopping from the central region to the right lead.
Starting from $n = 0$ with the GF of the left lead G^0, Dyson equation is used to compute the next GFs G^n for $n = 1, ..., L$. It is convenient to introduce a different GF, for numerical reasons:

$$\tilde{G}^n(\omega) := G^n(\omega + \epsilon^0_n), \tag{2.14}$$

with ϵ^0_n, the potential energy due to the electric field.
Then

$$\begin{aligned} \tilde{G}^n(\omega) &= g^n(\omega + \varepsilon^0_n) + g^n(\omega + \varepsilon^0_n) \big(t^2_{n-\frac{1}{2}} G^{n-1}(\omega + \varepsilon^0_n) \big) G^n(\omega + \varepsilon^0_n) \\ &= g(\omega - \varepsilon_n + \varepsilon^0_n) + g(\omega - \varepsilon_n + \varepsilon^0_n) \big(t^2_{n-\frac{1}{2}} \tilde{G}^{n-1}(\omega - \varepsilon^0_{n-1} + \varepsilon^0_n) \big) \tilde{G}^n(\omega) \\ &= g^n(\omega) + g^n(\omega) \big[t^2_{n-\frac{1}{2}} \tilde{G}^{n-1}(\omega + \Delta\varepsilon^0_{n-\frac{1}{2}}) \big] \tilde{G}^n(\omega) \\ \Delta\varepsilon^0_{n-\frac{1}{2}} &:= \varepsilon^0_n - \varepsilon^0_{n-1} \end{aligned}$$

LEFT TO RIGHT ITERATION
OF HALF INFINITE CHAIN

$$\tilde{G}^n(\omega) = g^n(\omega) + g^n(\omega) \big[t^2_{n-\frac{1}{2}} \tilde{G}^{n-1}(\omega + \Delta\varepsilon^0_{n-\frac{1}{2}}) \big] \tilde{G}^n(\omega) \tag{2.15}$$

(2.16)

The potential energy due to the electric field is

$$\varepsilon_n^0 = -E \cdot \{0, 0, 1, 2, \ldots, N_{cc}\} \qquad \text{for } n \in \{0, 1, \ldots, N_{cc}\}$$

so the first physical site of the central region endures the same potential energy as the last site of the left lead.
The total bias then is

$$V_{bias} = E * N_{cc}$$

For the advanced and retarded part the GF can simply be inverted as

ADVANCED/RETARDED PART OF LOCAL GF OF HALF-INFINITE SYSTEM

$$\left(\tilde{G}^n(\omega)\right)^{-1} = \left(g^n(\omega)\right)^{-1} - t^2_{n-\frac{1}{2}} \tilde{G}^{n-1}(\omega + \Delta\varepsilon^0_{n-\frac{1}{2}}) \ . \tag{2.17}$$

The Keldysh part is

KELDYSH PART OF LOCAL GF OF HALF-INFINITE SYSTEM

$$\left(\tilde{G}^n\right)^K(\omega) = \left(\tilde{G}^n\right)^r(\omega) \left[\left(\left(g^n\right)^r \right)^{-1} \left(g^n\right)^K \left(\left(g^n\right)^a \right)^{-1} + t^2_{n-\frac{1}{2}} \left(\tilde{G}^{n-1}\right)^K (\omega + \Delta\varepsilon^0_{n-\frac{1}{2}}) \right] \left(\tilde{G}^n\right)^a(\omega)$$

or by using Gl. (2.8), i.e.

$$\left(g^n\right)^K = v^2 \left(g^n\right)^r \left(g^n_b\right)^K \left(g^n\right)^a \ .$$

and get

KELDYSH PART OF LOCAL GF OF HALF-INFINITE SYSTEM

$$\left(\tilde{G}^n\right)^K(\omega) = \left(\tilde{G}^n\right)^r \left[v^2 \left(g_b(\omega)\right)^K + t^2_{n-\frac{1}{2}} \left(\tilde{G}^{n-1}(\omega + \Delta\varepsilon^0_{n-\frac{1}{2}})\right)^K \right] \left(\tilde{G}^n\right)^a \ .$$

Right to left

The next step is to construct the Green function for the half-infinite chain, starting from the right lead. Like for the left chain the iteration equation reads as

$$\begin{aligned} G^n &= g^n + g^n t_{n,n+1} G^{n+1} t_{n+1,n} G^n \\ &= g^n + g^n t^2_{n+\frac{1}{2}} G^{n+1} G^n \ . \end{aligned}$$

,
where the iteration starts from $N = N_c c$ and ends with $n = 1$. Forgetting what we have learned about the Green function so far G now denotes the GF of the half-infinte system that extends to the left. This is a different Green function than the one of the last section.

$$\begin{aligned} \tilde{G}^n(\omega) &= G^n(\omega + \varepsilon^0_n) \\ \tilde{G}^n(\omega) &= g^n(\omega + \varepsilon^0_n) + g^n(\omega + \varepsilon^0_n) t^2_{n+\frac{1}{2}} G^{n+1}(\omega + \varepsilon^0_n) \tilde{G}^n(\omega) \\ &= g(\omega - \varepsilon_n + \varepsilon^0_n) + g(\omega - \varepsilon_n + \varepsilon^0_n) t^2_{n+\frac{1}{2}} \tilde{G}^{n+1}(\omega - \varepsilon^0_{n+1} + \varepsilon^0_n) \tilde{G}^n(\omega) \\ &= \tilde{g}^n(\omega) + \tilde{g}^n(\omega) t^2_{n+\frac{1}{2}} \tilde{G}^{n+1}(\omega - \Delta\varepsilon^0_{n+\frac{1}{2}}) \tilde{G}^n(\omega) \ . \end{aligned}$$

The iteration begins with $n = N_{cc}$. Then

$$\tilde{G}^{n+1} = G^{n+1}(\omega + \varepsilon^0_{n+1}) = G^{\text{right lead}}(\omega + \varepsilon^0_{n+1}) = G^{\text{left lead}}(\omega)$$

The onsite energy of the left lead is set to zero. The iteration scheme for the right, as well as the left half-infinte system starts with $G^{\text{left lead}}(\omega)$. Due to inversion symmetry one finds

$$\overline{G}^n(\omega) = g^n(\omega) + g^n(\omega) t^2_{(n-\frac{1}{2})} \tilde{G}^{n-1}(\omega - \Delta\varepsilon^0_{(n-\frac{1}{2})}) \overline{G}^n(\omega) \ .$$

This is the same equation as that in Gl. (2.15), only the sign of the energy shift $\Delta\varepsilon_{n-\frac{1}{2}}$ is opposite. So the same code can be used for $\Delta\varepsilon_{n-\frac{1}{2}} \to -\Delta\varepsilon_{n-\frac{1}{2}}$ and in the end the indices of the GF are reverted, i.e.

$$\tilde{G}_n = \overline{G}_{N_{cc}-n} \ .$$

2.3.2 Connecting the two half-infinite chains at sites n and $n+1$

To formulate the Dyson equation that connects the two Green functions found in the previous sections one has to distinguish between the left half-infinite GF and the right half-infinite GF. The local GF at the end point of the left system that ends at position n is denoted by L^n and similarly the local GF of the right one that begins at site n is denoted by R^n Then the Dyson equation that connects the left

half-infinite system that ends at site n and the right one that begins at $n+1$ reads

$$\begin{aligned} G^{nn} &= L^n + L^n t_{n,n+1} R^{n+1} t_{n+1,n} G^{nn} \\ &= L^n + L^n \left[t^2_{n+\frac{1}{2}} R^{n+1} \right] G^{nn} \\ \left(G^{nn}\right)^{-1} &= \left(L^n\right)^{-1} - t^2_{n+\frac{1}{2}} R^{n+1} \ . \end{aligned}$$

Now the frequency argument of $G^{n,n}$ is shifted and the tilde GF:

$$\begin{aligned} \tilde{G}^{nn}(\omega) &= G^{nn}(\omega + \varepsilon^0_n) \\ &\Rightarrow \\ \left(\tilde{G}^{nn}(\omega)\right)^{-1} &= \left(\tilde{L}^n(\omega)\right)^{-1} - t^2_{n+\frac{1}{2}} \tilde{R}^{n+1}(\omega + \varepsilon^0_n - \varepsilon^0_{n+1}) \\ &= \left(\tilde{L}^n(\omega)\right)^{-1} - t^2_{n+\frac{1}{2}} \tilde{R}^{n+1}(\omega - \Delta\varepsilon^0_{n+\frac{1}{2}}) \ . \end{aligned}$$

is introduced.
For $G^{n,n+1}$ the Dyson equation is written differently

$$G^{n,n+1} = G^{n,n} t_{n+\frac{1}{2}} R^{n+1} \ .$$

The frequency shift is

$$\begin{aligned} \tilde{G}^{n,n+1}(\omega) &:= G^{n,n+1}(\omega + \varepsilon^0_n) \\ &= \tilde{G}^{n,n}(\omega) t_{n+\frac{1}{2}} \tilde{R}^{n+1}(\omega - \Delta\varepsilon^0_{n+\frac{1}{2}}) \ . \end{aligned}$$

Only the Keldysh component is needed which is

$$\left(\tilde{G}^{n,n+1}(\omega)\right)^K = t_{n+\frac{1}{2}} \left[\left(\tilde{G}^{n,n}(\omega)\right)^K \left(\tilde{R}^{n+1}(\omega - \Delta\varepsilon^0_{n+\frac{1}{2}})\right)^a + \left(\tilde{G}^{n,n}(\omega)\right)^r \left(\tilde{R}^{n+1}(\omega - \Delta\varepsilon^0_{n+\frac{1}{2}})\right)^K \right] .$$

2.3.3 Current calculation

With the Keldysh component of the connected GF the current can now be calculated in dependence of the potential energy due to the electric field.

2.3.4 Results and Analysis

To analyze the behaviour of a one-dimensional tight-binding Hubbard chain, the system was solved for different parameters. As the numerical calculations for the system built up on single-site clusters are cheaper and faster, it is a good way to start by doing calculations on that system before getting to bigger cluster sizes, to get a grasp of the behaviour. In the following section the results are presented. For all the calculations the hopping inside the leads t_{ll}, as well as the central region t_{cc} was set to 1. The hopping inside the bath chains t_{bb} as well as the Hubbard interaction U was changed. It has to be noted here that all energy values, like ω, U, E, etc. are given in units of the nearest neighbour hopping t_{cc}, which will be set to $t_{cc} = 1$ as mentioned above. The starting point for the analysis of the model was to set $U = 0$.

Non-interacting case

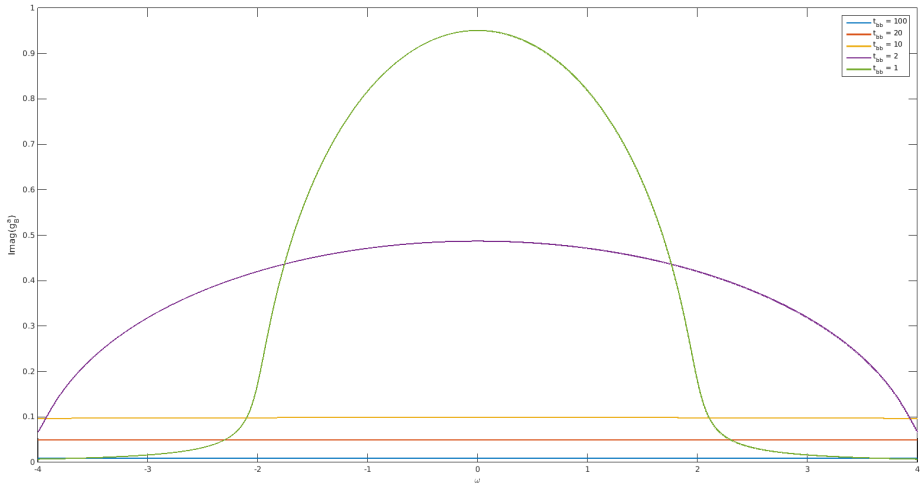

FIGURE 2.3: Imaginary part of the advanced bath Green function in dependence of the hopping parameter t_{bb} at $U = 0$. Semi-infinite chain (see eq. 2.12)

In figure 2.3 the imaginary part of the bath Green function is depicted. Concentrating on the green and purple curve one can see the bandwidth doubling with twice the hopping strength. The bandwidth is $2t_{bb}$. The half-circular behaviour shown in the figure is typical for a semi-infinte tight-binding chain. In the following figure the wide-band limit of the same Green functions are shown:

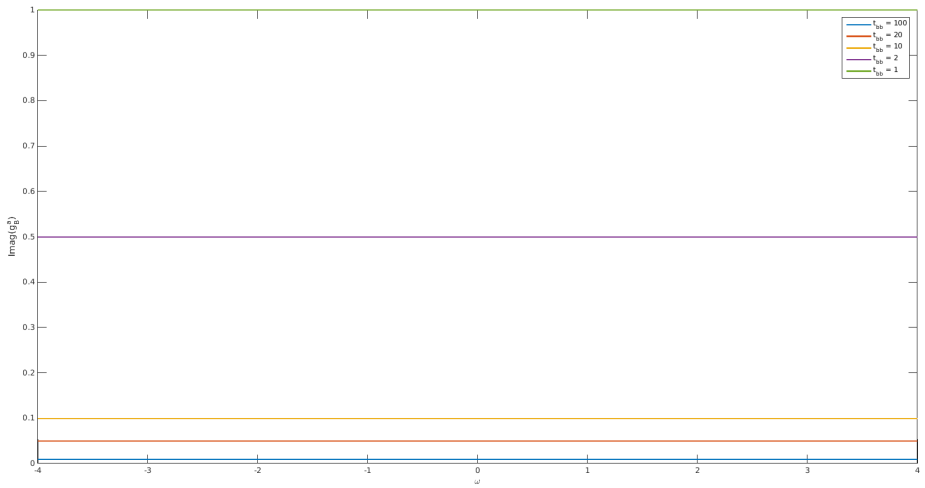

FIGURE 2.4: Imaginary part of the advanced bath Green function in dependence of the hopping parameter t_{bb} at $U = 0$. Wide-band limit (see eq: 2.13)

The reason why the limit is called wide-band limit becomes obvious by comparing these two figures. For higher hoppings, i.e. broader bandwidths the wide-band limit, which is just a constant imaginary Green function, is more exact than for smaller hoppings.
The system, more precisely the central region, in this thesis is finite. Therefore, at first, it was important to vary the size of the central region and compare the results with known results of an infinite system. In particular the work by Jong E. Han [13] was used to compare the finite system with the infinite tight-binding chain. Han found an analytical approximation for an electrical field driven current through an infinite tight-binding chain coupled to a fermionic bath:

THE HAN FORMULA

$$j_{Han} \approx \frac{4\Gamma t_{cc} E}{\pi(E^2 + 4\Gamma^2)} \tag{2.18}$$

with E the electric field, t_{cc} the hopping strength in the central region and $\Gamma = \frac{1}{t_{bb}}$ the damping constant of the fermionic bath chain. This formula is only viable in the strong-coupling limit $t_{cc} >> E, t_{cc} >> \Gamma$.

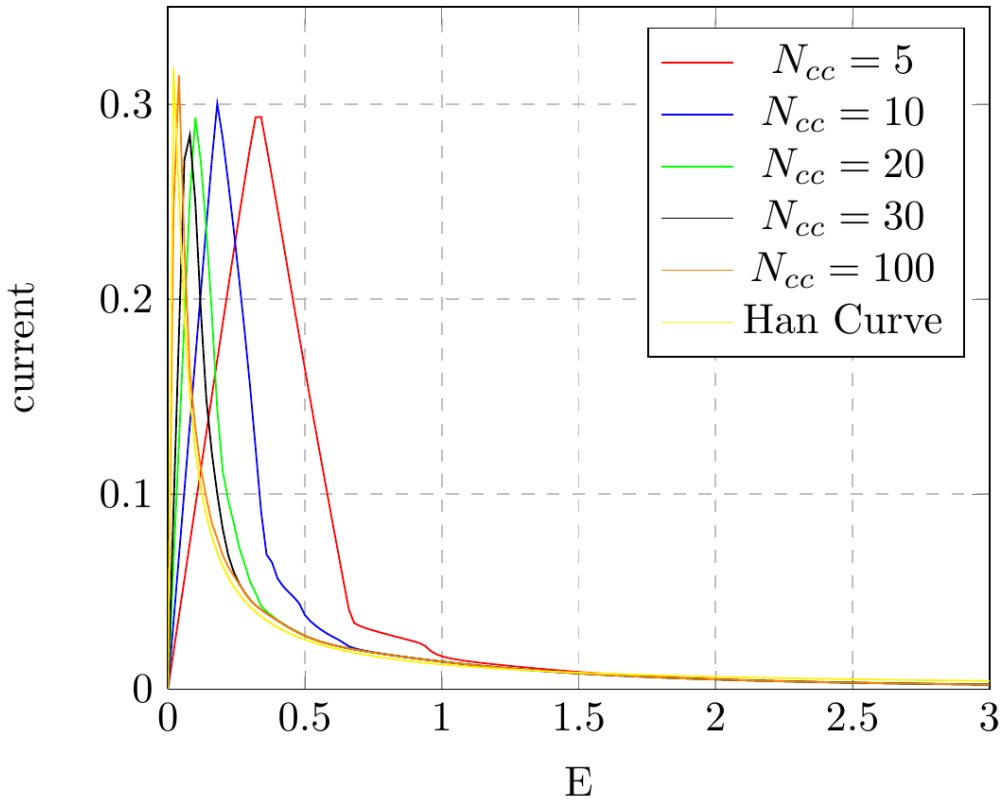

FIGURE 2.5: Different chain lengths at $t_{bb} = 100$ in comparison with the approximated formula by Han eq. 2.18

The Han formula is an approximation for an infinite tight-binding chain. Figure 2.5 shows, that smaller chains do not give the same current as the Han formula. While all chain lengths show qualitatively more or less the same behaviour, in terms of one sharp peak, the peak height as well as the position of the peak varies. As these calculations have been done for $U = 0$, the chain shows, independently of its length, a metallic behaviour with a linear response.
Up to this point all calculations were done using the formula for the semi-infinite tight-binding chain (eq. 2.12) to express the bath chain Green functions. As the computation time for the wide-band limit is lower, it has to be checked, if the two different approaches for the bath chain Green functions give comparable results for the current.

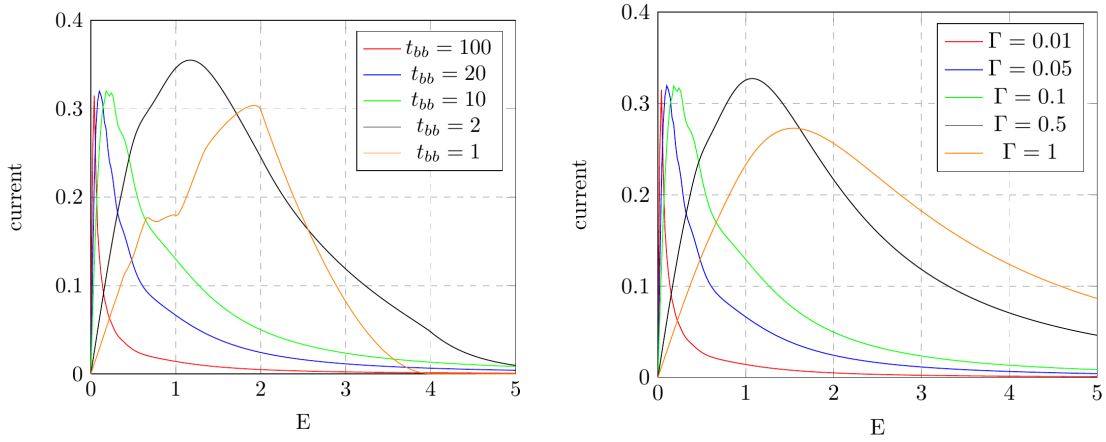

(A) Semi-infinite chain (see eq. 2.12)

(B) Wide-band limit (see eq. 2.13)

FIGURE 2.6: $N_{cc} = 100$, $U = 0$. Current in the center of the chain at different hopping strengths inside the bath chains.

When comparing figures 2.6a and 2.6b it is imminent that the wide-band limit is not valid for smaller hoppings anymore. This conclusion is a confirmation for the statement made previously when comparing the Green functions of the bath chains directly in the semi-infinite tight-binding and wide-band limit approach (see figures 2.3 and 2.4).
Although the wide-band limit requires less computation time, the realisation of fermion reservoir bath chains by using the semi-infinte tight-binding approach (eq. 2.12) seems to be closer to reality and will therefore mostly be used in this work, if not indicated otherwise.
It is obvious that different hopping strengths/damping constants in the fermionic bath chains give different current curves. The position of the maxima changes as well as the width of the peaks. However, they qualitatively all show a similar behaviour, with a linear increasing current for lower field energies, one maximum and a decreasing behaviour at higher energy values. The position of the maxima as well as the reason for the linear increase and the decrease will be discussed in this chapter.

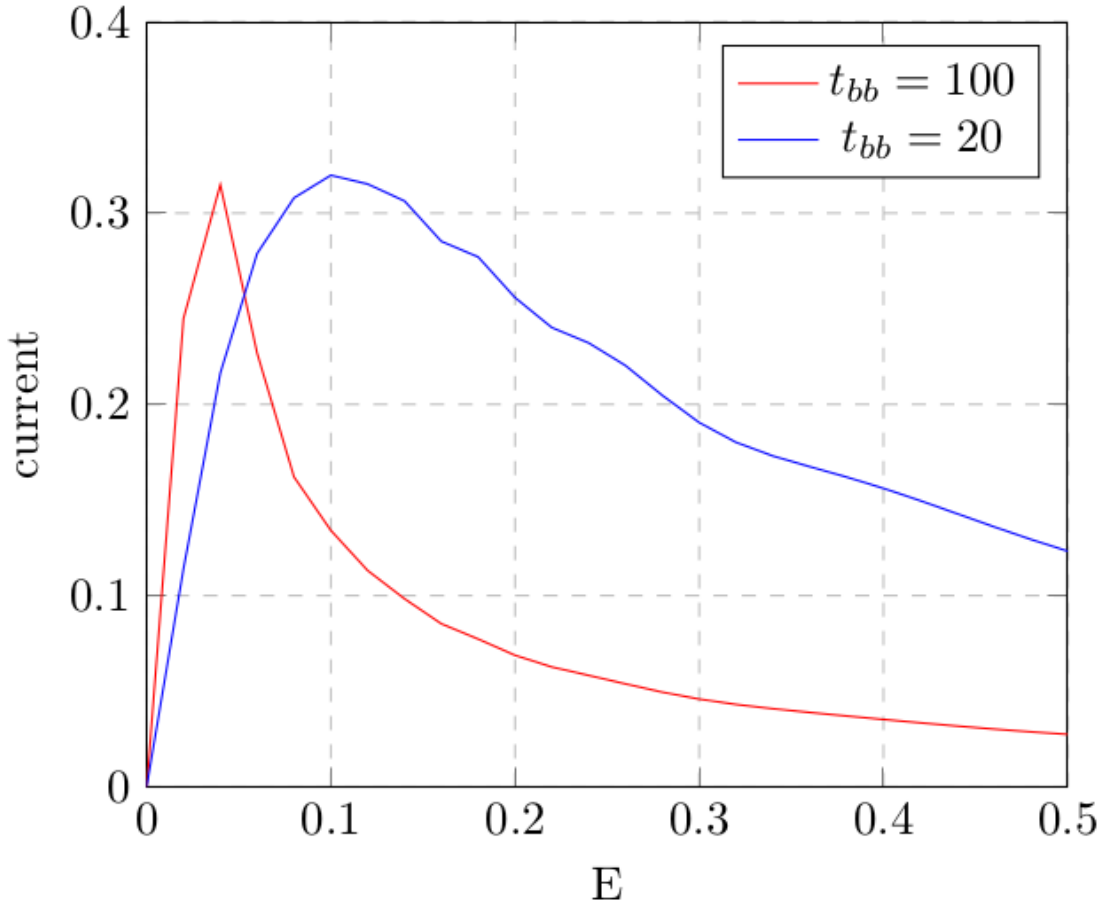

FIGURE 2.7: Zoomed-in picture of the current-field curve at $t_{bb} = 100$ and $t_{bb} = 20$, corresponding to $\Gamma = 0.01$ and $\Gamma = 0.05$ in the wide-band limit.

From 2.7 one can determine the maxima of the current curve, with respect to the external electric field. In this figure the hopping strengths in the fermionic bath chains were chosen to be in the wide-band limit regime. One can see the maximum of the curve for the $t_{bb} = 20 \hat{=} \Gamma = 0.05$ is at 0.1 which is 2Γ. The maximum of the curve with hopping parameter $t_{bb} = 100 \hat{=} \Gamma = 0.01$ is at 0.02.
This goes in accordance with eq. 2.18. It also ratifies the importance of having those fermionic bath chains coupled to the physical sites. No bath chain would mean a damping constant of $\Gamma = 0$ which would result in a zero current density, as the 'maximum' for the current density would be at $E = 0$, which gives a current density of $j = 0$.
For small values of E, up to the maxima of the curves depicted in 2.7, the current density shows an Ohm-like linear behaviour $j(E) \propto E$. However at bigger values of E, the current density decreases and does so differently for differing damping constants Γ. The explanation can be found in the gaining influence of Bloch oscillations at higher electric field strengths. The gain in energy of electrons moving along the chain is proportional to the electric field strength, however the dissipation is dependent on the damping parameter. The decreasing current density is

due to the dissipation mechanism not being able to suppress the Bloch oscillations at higher field strengths. Comparing the curves for different damping constants in 2.6b and 2.6a indicates that the different hopping strengths in the bath chains give in fact weaker or stronger dissipation. The current density decays way faster for higher hopping parameters, or equivalently weaker damping parameters.
As a summary: A chain length of $N_{cc} = 100$ is necessary to achieve results close to the analytical approximation for an infinite tight-binding chain. The wide-band limit approach for the reservoir bath chains is only viable for hopping strengths $t_{bb} \geq 10$, or in terms of the damping parameter $\Gamma \leq 0.1$

Interacting case

With the analysis done for the non-interacting case (i.e. $U = 0$) it is now possible to examine the system in presence of an interaction. For the non-interacting case the chain showed, independently of chain size and hopping-strength inside the fermionic reservoir bath chains, a metallic behaviour.
The first calculation was made with parameters $U = 1$, $t_{bb} = 100 \hat{=} \Gamma = 0.01$ and $N_{cc} = 50$. While for the non-interacting case the onsite-energy $\epsilon = 0$ trivially, in the case of interacting chains, one has to specify ϵ_0. For the calculations in this work the onsite energy mostly is set to $\epsilon_0 = \frac{U}{2}$, if not indicated otherwise. This corresponds to a half-filled band, meaning there are as many electrons in the system, as there are lattice sites.

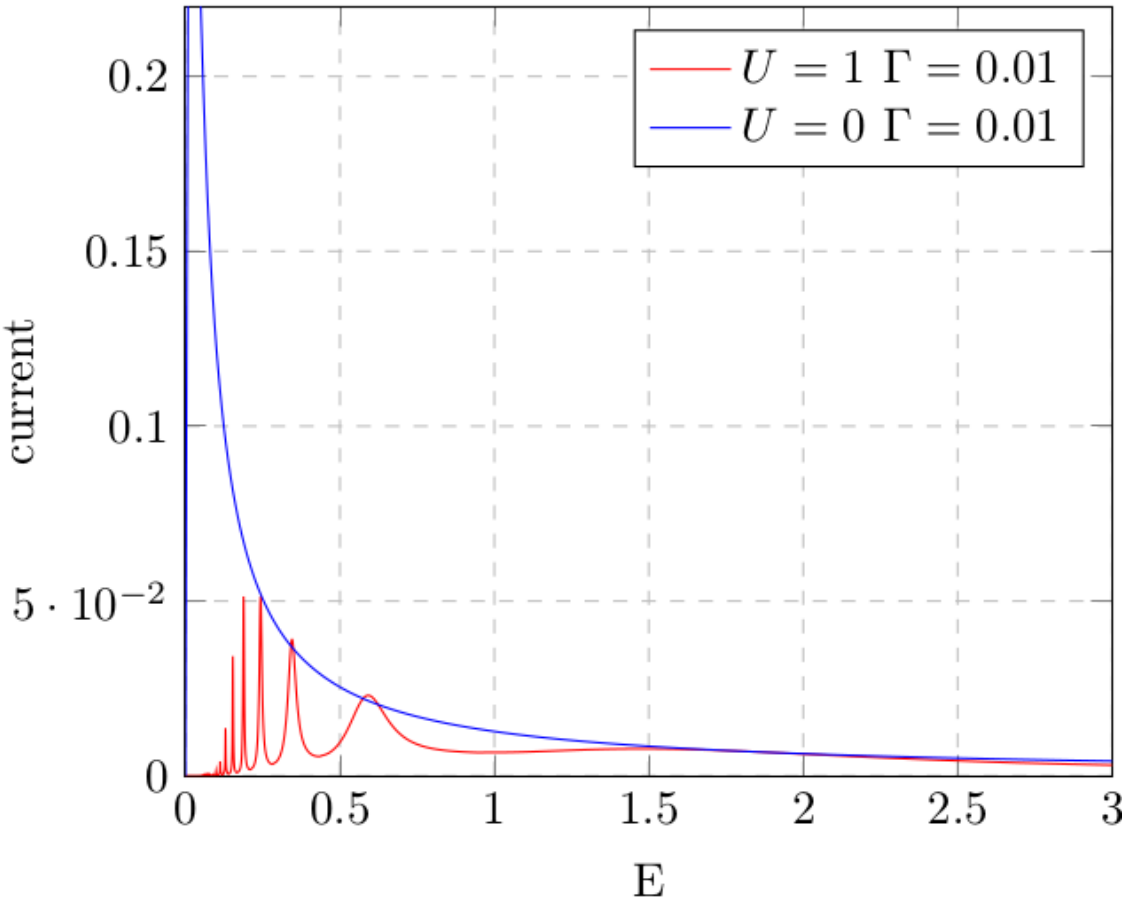

FIGURE 2.8: Current density with respect to the external electric field. A damping parameter of $\Gamma = 0.01$ was chosen. The chain length is $N_{cc} = 50$. The blue curve is the analytical result for $U = 0$

Looking at 2.8 two major differences to the non-interacting case are obvious. Firstly, the current stays zero at small values of E and secondly, there are oscillations in the current curve.
As already mentioned before, the dissipation mechanism, provided by the application of artificial fermionic bath chains to the physical sites, suppresses the occuring oscillations. To explain the oscillations it is important to give a brief understanding of Wannier-Stark resonances.

Wannier-Stark ladder and Zener tunneling

The so-called Wannier-Stark problem deals with single particles in a one dimensional periodic potential under the influence of a static force. [14] [10]
The Hamiltonian is

$$H_W = \frac{p^2}{2m} + V(x) + Fx, V(x+d) = V(x), \tag{2.19}$$

where F is the static external force, induced by an external field (e.g. an electric field like in this thesis). The external field destroys the translational symmetry of

the Hamiltonian (without the force). Given an arbitrary eigenstate, which satisfies

$$H_w \left|\Psi\right\rangle = E_0 \left|\Psi\right\rangle, \tag{2.20}$$

one can construct a so-called **Wannier-Stark ladder** with energies $E_l = E_0 + ldF$. Superpositions of the states belonging to these energies have oscillatory evolutions with the so-called Bloch period

$$T_B = \frac{2\pi\hbar}{dF}. \tag{2.21}$$

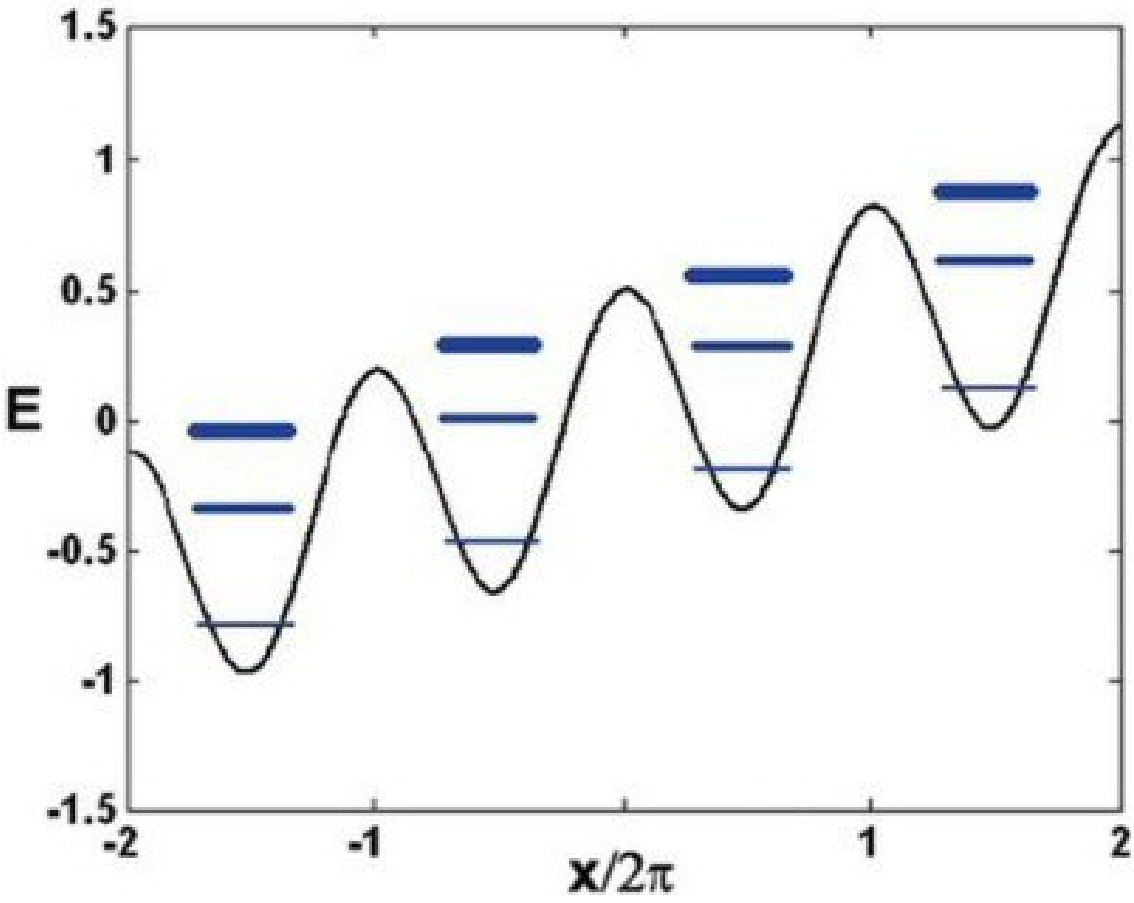

FIGURE 2.9: Schematic illustration of the Wannier-Stark ladder. The thickness of lines indicates the width of of the levels (their instability). Figure taken from [14]

According to [43] [10] [14] [5] the Wannier-Stark model enables resonance tunneling processes that can be observed for the interacting systems.
While it has been thought that the periodic potential has to meet certain conditions [12] [11] it was shown recently that any periodic potential causes these resonances [35].
The next step is to look at larger values of U as well as observe the influence of the hopping inside the fermionic bath chains. As already mentioned the energy loss due to dissipation is proportional to the damping parameter Γ.

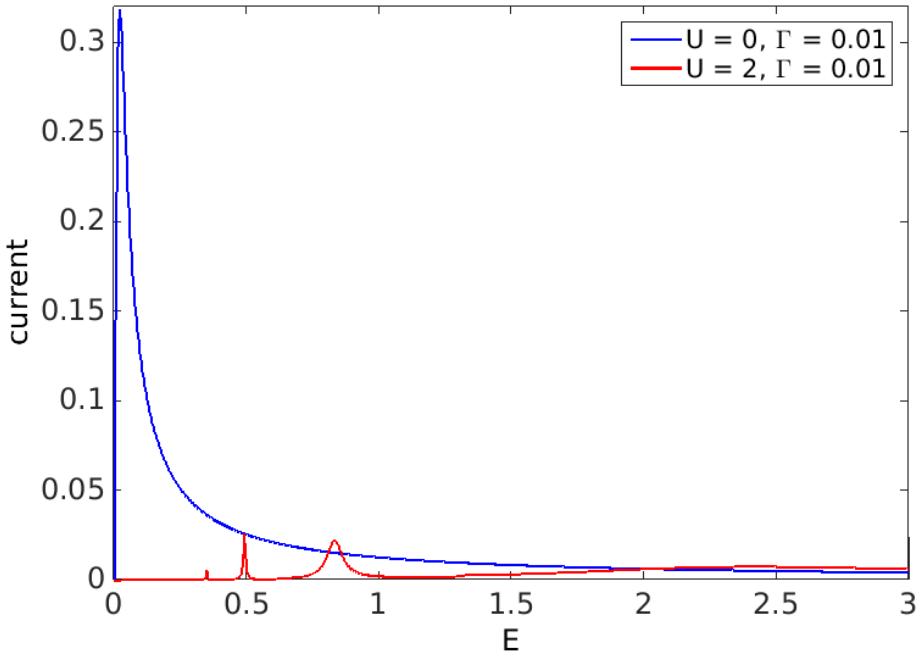

FIGURE 2.10: Current density for $U = 2$. The blue curve is the analytical solution for $U = 0$.

Looking at figure 2.10 the stronger interaction leads to an even bigger suppression of the current density. The isolating regime in the beginning is bigger than for the $U = 1$ interaction. As shown in the next section the cluster size does have an influence on the current for $U \neq 1$.

2.4 2-site cluster

CPT is a great techinque because it allows huge systems to be split up into smaller ones, which can be solved exactly, and put together again to reproduce the full system. The bigger the cluster size is the better, as the exact diagonalisation is used for a greater part of the system. Therefore, the next step will be to solve clusters of two neighbouring physical sites, connected to their respective fermionic baths and couple them via Dyson equation to build up the finite tight-binding chain.
The first step is to determine the retarded (or advanced) Green function of the isolated cluster, consisting of two physical sites of the chain. This is done by setting up the Hamiltonian for a tight-binding Hubbard model with two sites, solving it by exact diagonalisation and applying the Lehmann representation eq. 1.19 to calculate the isolated cluster Green function $g^0(\omega)$. Unlike in the previous

section, where there was only one site in the cluster, $g^0(\omega)$ is a 2x2 matrix and not a vector anymore.

$$g^0(\omega_1) = \begin{pmatrix} g^0_{11}(\omega_1) & g^0_{12}(\omega_1) \\ g^0_{21}(\omega_1) & g^0_{22}(\omega_1) \end{pmatrix} \tag{2.22}$$

The indices stand for the sites of the cluster. $g^0_{11}(\omega)$ is the Green function of the isolated cluster projected onto the first physical site, inside the cluster, $g^0_{12}(\omega)$ is in-between sites 1 and 2 and so on.
Applying an electric field E yields a potential $\epsilon(E)$ at the cluster sites in the non-equilibrium, so therefore a correction has to be made to isolated cluster GF.

$$[\tilde{g}^0(\omega)]^{-1} = [g^0(\omega)]^{-1} - \begin{pmatrix} \epsilon_1(E) & 0 \\ 0 & \epsilon_2(E) \end{pmatrix} \tag{2.23}$$

$\tilde{g}^0(\omega)$ now is the Green function of the isolated cluster under the influence of the homogenous electric field. This GF now has to be coupled to its respective bath chains $g_b(\omega)$ by using Dyson's equation. One has to keep in mind that the bath chains also need to be shifted in energy-space to be correctly connected to their inherent physical site.
Note: The Green function of the isolated cluster has to be calculated only once. However the correction has to be made for every value of E. The Dyson equation to couple the bath chains to the cluster is

$$[\tilde{g}(\omega)]^{-1} = [\tilde{g}^0(\omega)]^{-1} - T_{12} g_b(\omega) T_{21}, \tag{2.24}$$

with

$$T_{12} = \begin{pmatrix} 0 & t_{cb} \\ 0 & 0 \end{pmatrix} \tag{2.25}$$

and

$$T_{12} = \begin{pmatrix} 0 & 0 \\ t_{cb} & 0 \end{pmatrix} \tag{2.26}$$

the coupling matrices that contain the hopping parameters into the bath chain.
$g_b(\omega)$ is a 2x2 matrix containing the two Green functions for the bath chains, shifted in energy space, in the diagonal. Similar to the 1-site cluster these GFs can be calculated by using the analytical formula for the

SEMI-INFINTE TIGHT-BINDING CHAIN [6]

$$g_0^{b.a}(\omega) = \frac{\omega}{2t_{bb}^2} \pm \frac{1}{t_{bb}} \sqrt{(\frac{\omega}{2t_{bb}})^2 - 1} \tag{2.27}$$

or using the

WIDE-BAND LIMIT

$$g_0^{b.a}(\omega) = i\Gamma \tag{2.28}$$

The Keldysh component can be calculated by using eq. 2.11. Once again it has to be noted that the chemical potential appears by calculating the Keldysh part, as the Fermi-function makes an appearence. As before the chemical potential was set to a value to induce half-filling.
$\tilde{(}g)(\omega)$ includes the retarded, advanced and Keldysh part:

$$g_b(\omega, E) = \begin{pmatrix} \begin{pmatrix} g_b^r(\omega - \epsilon_1(E) & 0 \\ 0 & g_b^r(\omega - \epsilon_2(E) \end{pmatrix} & \begin{pmatrix} g_b^K(\omega - \epsilon_1(E) & 0 \\ 0 & g_b^K(\omega - \epsilon_2(E)) \end{pmatrix} \\ 0 & \begin{pmatrix} g_b^a(\omega - \epsilon_1(E) & 0 \\ 0 & g_b^a(\omega - \epsilon_2(E) \end{pmatrix} \end{pmatrix} \tag{2.29}$$

With the cluster now coupled to its bath chains the next step will be to start the iteration to form the whole chain. Once again it is necessary to do an iteration from left to right as well as from right to left and couple those semi-infinte chains together.

Left and right iteration

Starting from the left lead, a semi-infinite tight binding chain, the first cluster will be coupled to the lead. We define the electric field to be zero for the left lead as well as the first physical site of the chain. The Dyson equation yields

$$G_{11}^L = g_{11} + g_{11} T_{10}^L G_{01}^L \tag{2.30}$$
$$G_{01}^L = g_{00} T_{01}^L G_{11}^L, \tag{2.31}$$

with G_{11}^L being the Green Function of the central cluster coupled to the left lead, G_{01}^L the Green function in between the left lead and the central cluster and g_{00} the GF of the boundary site of the left lead. T_{01}^L is the coupling matrix that is zero everywhere, except for one off-diagonal entry, where the hopping parameter t_{lc} stands to couple the lead to the central cluster. All hoppings (except for the ones inside the fermionic bath chain) are set to 1.
Reintroducing the dependency of ω and E and explicitly writing the desired Green function, the Dyson equation can be written as

$$[G^L(\omega, E)]^{-1} = [\tilde{g}(\omega, E)]^{-1} - T_{10}^L g_{00}^L(\omega, E) T_{01}^L \tag{2.32}$$

One has to note that for the inverted equilibrium cluster Green function $[g^0(\omega)]^{-1}$ the Keldysh component can be set to zero, giving the four-component Geen function

$$[g^0(\omega, E)]^{-1} = \begin{pmatrix} [g_0^r(\omega, E)]^{-1} & 0 \\ 0 & [g_0^a(\omega, E)]^{-1}, \end{pmatrix} \tag{2.33}$$

where $g_0^r(\omega, E)$ is the retarded part of the GF and $g_0^a(\omega, E)$ the advanced. Both of these Green functions have the dimension 2x2.
When coupling the lead to the central cluster one does in fact gain another semi-infinite chain that has grown by one cluster. As for the 1-site cluster one can repeat this process until all physical sites of the chain are iteratively connected. The important part is to shift the semi-infinte chain by $\omega_{shift} = 2E$ before coupling them and demand that the obtained Green function is equal to that of the unshifted chain.

$$[G^L(\omega, E)]^{-1} = [g^0(\omega, E)]^{-1} - T_{10} g_b(\omega) T_{01} + T_{10}^L g_{00}^L(\omega + \omega_{shift}, E) T_{01}^L \tag{2.34}$$

For the right to left iteration the process is exactly the same however one starts at the right lead and adjusts the energy shift accordingly.
The last step will be to connect the two chains via Dyson equation:

$$[G(\omega, E)]^{-1} = [g^0(\omega, E)]^{-1} - T_{10} g_b(\omega) T_{01} - T_{10}^L g^L(\omega + \omega_{shift}, E) T_{01}^L - T_{10}^R g^R(\omega - \omega_{shift}, E) T_{01}^R \tag{2.35}$$

which again yields a 2x2 matrix. The current can now be calculated by using eq. 1.76.

2.4.1 Results

As for the 1-site cluster the chain was solved for different parameters.
The hopping inside the lead chains, as well as the central region was once more set to $t_{lc} = t_{cl} = t_{cc} = t_{ll} = 1$ while the hopping strength in the bath chains varied. If not indicated otherwise eq. 2.27 was used to calculate the bath Green function and not the wide-band limit eq. 2.28.

Non-interacting case

First, the non-interacting case, i.e. $U = 0$, has been calculated. According to [28] the cluster size only plays a role for values $U \neq 0$, so the non-interacting case should look similar to what has been found for the 1-site cluster.

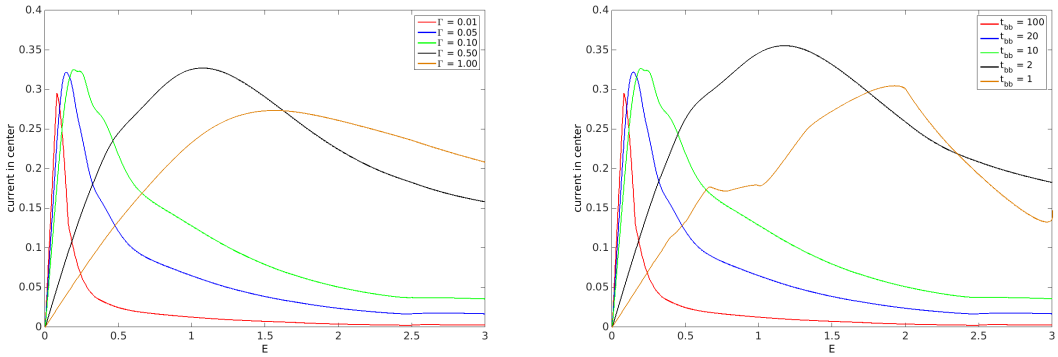

(A) Semi-infinite chain (see eq. 2.12) (B) Wide-band limit (see eq. 2.13)

FIGURE 2.11: $N_{cc} = 50$, $U = 0$. Current in the center of the chain at different hopping strengths inside the bath chains.

Like for the 1-site cluster calculations the differences between the wide-band limit and the semi-infinite tight binding chain for the fermionic bath chains was looked at. The results are very similar to the 1-site cluster results, in terms of position of peaks and the behavior of the current. Independent of the hopping strength all chains show a metallic behaviour, with a linear, ohm-like rise of current for lower values of the electric field, up unto a maximum value. This behaviour has already been explained in the previous chapter. Indeed, the cluster size does not seem to have an influence on the calculations in the non-interacting case.
Future calculations will be done at a strong hopping in the bath (i.e. $t_{bb} = 100, \Gamma = 0.01$ as the results for the wide-band limit and the semi-infite tight-binding chain are the same. Once again the maxima of the current curves are at values 2Γ.

Interacting case

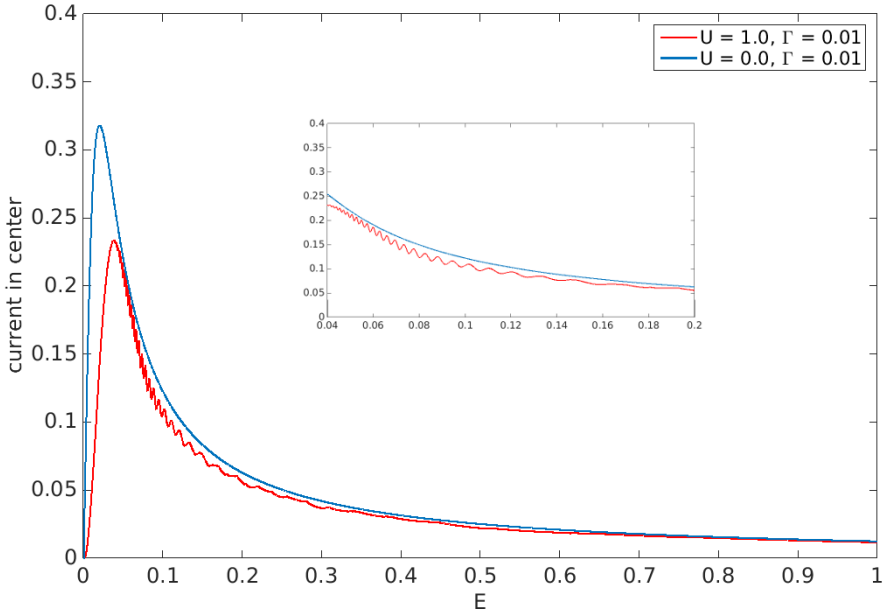

FIGURE 2.12: Current density for $U = 1$. The blue curve is the analytical solution for $U = 0$.

In the figure above the current calculation for $U = 1$ is shown for the 2-site cluster. The interesting region between values of $E = 0.04$ to $E = 0.2$ is magnified in the subplot. Comparing the results with the ones of the 1-site cluster the difference is striking.
Oscillations do occur, allthough unlike for the 1-site cluster, the chain still shows metallic behaviour with a linear rise in current for lower values of the electric field. The maximum is damped as well, compared to the non-interacting result, however not as much as for the 1 site cluster. The origin of the resonant structures can be traced back to the occurrence of short-range anti-ferromagnetic order [28].

For $U = 2$ the same parameters ($\Gamma = 0.01$, all other hoppings set to 1) were used to calculate the current curve.

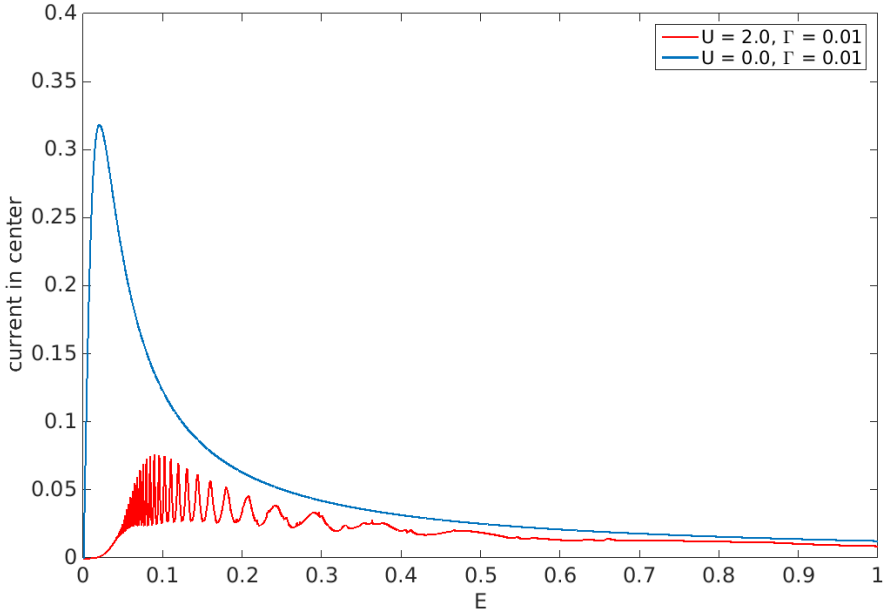

FIGURE 2.13: Current density for $U = 2$. The blue curve is the analytical solution for $U = 0$.

Once again it is obvious that the cluster size does play a role. While for the 1 site cluster the current was suppressed essentially, the result for the 2-site cluster shows an oscillating behaviour, allthough the current is non-zero after the isolating gap at low energy values.
At bigger cluster sizes the behaviour changes further, allthough this has been analysed in previous works [28]. In this work however, the influence of self-energy changes according to VCA is investigated to see if it is possible to deal with the oscillating behaviour at higher values of U.

Chapter 3

Variational cluster approximation

3.1 Introduction

As already discussed previously, the understanding of simple systems like the Hubbard model and especially its behaviour in non-equilibrium conditions has been a very important part of many-body physics for the last few decades. It has already been stated that CPT provides a simple, yet viable tool to solve very big to infinite models, without having to spend a large amount of resources. However, CPT as applied up to now in this work, faces limitations, like its lack of possibility to describe broken-symmetry states. [38] Luckily CPT is not the end of the road. The idea is to upgrade the method by introducing a set of parameters which are altered self-consistently throughout the calculations. The upgraded method of CPT is called **variational cluster approximation**.
Methods have been developed that use the self-energy Σ as a dynamic variable. A functional $\Omega(\Sigma)$ is constructed which can be shown to be stationary at the physical self-energy, leading to the self-energy-functional theory (SFT) [32].
It has to be noted that next to VCA there have been many quantum-cluster theories [26], developed in the past years. Examples are the cluster extansions of the dynamical mean-field theory, like the dynamical cluster approximation [16] and the cellular dynamic mean-field theory [20] [24].
Considering a Hamiltonian $H = H_0(t) + H_1(U)$, with one-particle hopping parameter t and interaction parameter U, this grand potential is

$$\Omega(\Sigma) = F(\Sigma) + \mathit{Trln}(G_0^{-1} - \Sigma)^{-1}, \tag{3.1}$$

with $G_0 = (\omega + \mu - t)^{-1}$ the free Green function of the original model at frequency ω and $F(\Sigma)$ the Legendre transform of the universal Luttinger-Ward functional [21] [33] [32].
Using the universality the functional can be obtained within the subspace, of self-energies $\Sigma = \Sigma(p')$, with a modified set of parameters p' [1].
Now the stationary solution has to be found. This is characerized by the condition

$$\frac{\partial \Omega}{\partial p'} = 0. \tag{3.2}$$

So the VCA alters the self-energy of a (in this case) Hubbard system by introducing a modified set of parameters p'. This set of parameters could include the chemical potential, the hopping strength within, or without a Hubbard chain, the on-site energies and much more.

The idea of this thesis is to introduce an auxilary bath site to the system, which is coupled to the physical site within the chain by a hopping parameter t_a and has the on-site energy ϵ_a. These two parameters correspond to the set of parameters p' mentioned above. The exact method will be discussed later on in this chapter.

3.2 Model and method

The model used for the variational cluster approximation is basically the same as in chapter 2. The difference between the two models is the addition of a bath site, coupled to every physical site in the central region.

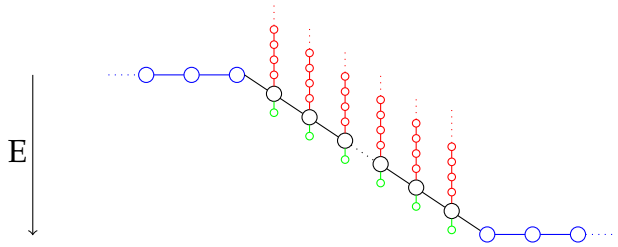

FIGURE 3.1: A finite Hubbard chain with correlated electrons in a homogenous E field attached to leads. One bath site is coupled to every physical site in the central region.

The Hamiltonian for this system is

$$H = H_0 + H_1 \tag{3.3}$$

With

$$H_0 = H_0^{cl} + T_C + T_B \tag{3.4}$$

H_0^{cl} is the Hamiltonian of the isolated cluster, consisting of the sites along the tight-binding chain of the central region, as well as the sites inside the (red) bath chains. T_C is the hopping term along the central region and T_B the hopping into the (red) bath chains.
Now the VCA bath site has to be added via the Hamiltonian H_A. As VCA is only used to alter the self-energy of the system [19], the Hamiltonian H_A needs to be subtracted again. So the Hamiltonian of the unperturbed system reads as

$$H_0 = H_0^{cl} + H_A + T_B + T_C - H_A. \tag{3.5}$$

3.5 describes an isolated 2 site cluster, consisting of a physical site and a VCA bath site. Adding the interaction term of the Hamiltonian the full Hamiltonian of the system reads as

$$H = \underbrace{H_0^{cl} + H_A + H_1}_{\Rightarrow g_{cl}} - \underbrace{H_A + T_B + T_C}_{one-particle-terms} \tag{3.6}$$

To solve the problem the CPT formalism is used. The central equation to obtain the Green function of the full system is

$$G^{-1} = (g_{cl})^{-1} + H_A - T_B - T_C \tag{3.7}$$

As already hinted in 3.6, g_{cl} is the Green function of the physical site and the VCA bath site, without correction, i.e. the VCA bath site is not subtracted.
To keep track of the Green functions used to obtain the full Green function of the whole system it is wise to introduce the following notation:

CORRECTED GREEN FUNCTION OF THE ISOLATED CLUSTER

$$\tilde{g}_{cl} = \left[(g_{cl})^{-1} + H_A\right]^{-1} \tag{3.8}$$

CORRECTED GREEN FUNCTION OF THE ISOLATED CLUSTER COUPLED TO THE SEMI-INFINITE BATH CHAIN

$$\overline{g_{cl}} = \left[(\tilde{g}_{cl})^{-1} - T_B\right]^{-1} \tag{3.9}$$

FULL GREEN FUNCTION

$$G = \left[(\overline{g_{cl}})^{-1} - T_C\right]^{-1} \tag{3.10}$$

The Green function g_{cl} of the isolated cluster can be determined using the Lehmann representation. The problem at hand is that of a Hubbard-like model with two sites. The Hubbard-interaction U only acts on the physical site. The hopping between physical and VCA bath site is t'_{cb}. The on-site energy on the physical site is $\epsilon_0 = -\frac{U}{2}$ and the onsite energy on the VCA bath site is ϵ_b. The Hamiltonian for this 2-site problem is

$$H_{cl} = -t'_{cb} \sum_{\sigma} (\hat{c}^{\dagger}_{1\sigma} \hat{c}_{2\sigma} + h.c.) + U \hat{n}_{1\uparrow} \hat{n}_{1\downarrow} + \epsilon_0 \sum_{\sigma} \hat{n}_{1\sigma} + \epsilon_b \sum_{\sigma} \hat{n}_{2\sigma} \tag{3.11}$$

As particle-hole-symmetry shall be given, the on-site energy of the VCA bath site ϵ_b must be set to zero.
The cluster Green function g_{cl} is therefore a 2x2 matrix. For future calculations, the only thing of interest is the Green function of the physical bath site. In terms of CPT, the Dyson equation for the corrected Green function of the cluster is

$$\tilde{g}_{cl} = g_{cl} + g_{cl} H_A \tilde{g}_{cl} \tag{3.12}$$

Multiplying $(\tilde{g}_{cl})^{-1}$ from the right side and $(g_{cl})^{-1}$ from the left side yields

$$(\tilde{g}_{cl})^{-1} = (g_{cl})^{-1} + H_A. \tag{3.13}$$

Inversion of 3.13 gives exactly 3.8.
At this point the full 2x2 matrix is not needed anymore for future calculations. $\tilde{g}_{cl}^{cc}$ now denotes the corrected Green function of the isolated cluster at the physical site. The construct $\tilde{g}_{cl}^{cc}$ is now a vector.
The next step is adding the semi-infinite bath chains to the cluster Green function. The Dyson equation reads as

$$\overline{g_{cl}}^{cc} = \tilde{g}_{cl}^{cc} + (\tilde{g}_{cl} T_B \overline{g_{cl}})^{cc} \tag{3.14}$$

and as the Green functions in 3.14 are vectors, this equation can be written as

$$\overline{g_{cl}}^{cc} = \tilde{g}_{cl}^{cc} + \tilde{g}_{cl}^{cc} t_{cb}^2 \overline{g_{cl}}^{cc} \tag{3.15}$$

with t_{cb} the hopping paramter connecting the physical site to the semi-infinite bath chain.
Finally this construct has to be coupled to the next cluster. Once again the Dyson equation reads as

$$G^{cl} = \overline{g_{cc}} + \overline{g_{cc}} T_C \overline{g_{cc}}, \tag{3.16}$$

where again only the part projected on the physical site is of relevance, which is indicated by using the indices g_{cc} according to the notation above.
VCA demands that the self-energy of the cluster is changed in a way that the Green function with all many-body effects gets as similar to the Green function of the isolated cluster as possible. Therefore one needs a

SELF-CONSISTENCY CONDITION [19]

$$\int \frac{d\omega}{2\pi} Tr\left(\frac{\partial (g_{0cc})^{-1}}{\partial \mathbf{p}} \tilde{g}_{cc} - G_{cc}\right)^K = 0 \tag{3.17}$$

or further

$$\int \frac{d\omega}{2\pi} \left[\frac{\partial ((g_{0cc})^{-1})^R}{\partial \mathbf{p}} (\tilde{g}_{cc} - G_{cc})^K + \frac{\partial ((g_{0cc})^{-1})^K}{\partial \mathbf{p}} (\tilde{g}_{cc} - G_{cc})^a\right] = 0 \tag{3.18}$$

Instead of deriving the Green function one can also use the self-energy

$$\int \frac{d\omega}{2\pi} \left[\frac{\partial ((\Sigma)^{-1})^R}{\partial \mathbf{p}} (\tilde{g}_{cc} - G_{cc})^K + \frac{\partial ((\Sigma)^{-1})^K}{\partial \mathbf{p}} (\tilde{g}_{cc} - G_{cc})^a\right] = 0 \tag{3.19}$$

The first step in the VCA process is now to calculate the self-energy for the first time.

SELF ENERGY

$$\Sigma_0 = \omega + i0^+ - (\tilde{g}_{cl}(t'_{cb}, \epsilon_b))^{-1} + \epsilon_0 \tag{3.20}$$

One has to keep in mind that the Green function $\tilde{g}_{cl}$ is calculated by solving the Hamiltonian of a 2-site tight-binding problem with a hopping of t'_{cb} between the physical site and the auxilary bath site. The on-site energy of the auxilary site is ϵ_b.
Now the hopping parameter t'_{cb} is changed by a value dt_{cb} and the self-energy recalculated.

SELF ENERGY
FOR HOPPING PARAMETER $t'_{cb} + dt_{cb}$

$$\Sigma_p = \omega + i0^+ - (\tilde{g}_{cl}(t'_{cb} + dt_{cb}, \epsilon_b))^{-1} + \epsilon_0 \tag{3.21}$$

with the differential of the self energy

$$d\Sigma_t = \frac{\Sigma_p - \Sigma_0}{dt_{cb}} - \tag{3.22}$$

The same has to be performed for the other variational parameter ϵ_b

SELF ENERGY
FOR ONSITE ENERGY PARAMETER $\epsilon_b + d\epsilon_b$

$$\Sigma_p = \omega + i0^+ - (\tilde{g}_{cl}(t'_{cb}, \epsilon_b + d\epsilon_b))^{-1} + \epsilon_0 \tag{3.23}$$

and the differential of the self energy

$$d\Sigma_\epsilon = \frac{\Sigma_p - \Sigma_0}{d\epsilon_b} - \tag{3.24}$$

Now eq. 3.19 can be used to calculate the cost function that has to be minimized to gain the optimal VCA parameters. To keep the equation clean the integrals are split up into 4 parts:

$$(s_1)^{RK} = \int \frac{\omega}{2\pi} d\Sigma_t^R(\omega + d\omega) G_{cl}^K(\omega) \tag{3.25}$$

$$(s_1)^{KA} = \int \frac{\omega}{2\pi} d\Sigma_t^K(\omega + d\omega) G_{cl}^A(\omega) \tag{3.26}$$

$$(s_2)^{RK} = \int \frac{\omega}{2\pi} d\Sigma_t^R(\omega + d\omega) \tilde{g}_{cl}^K(\omega) \tag{3.27}$$

$$(s_2)^{KA} = \int \frac{\omega}{2\pi} d\Sigma_t^K(\omega + d\omega) \tilde{g}_{cl}^A(\omega) \tag{3.28}$$

where the differential of the self-energy had to be shifted in energy space to match the respective position of the cluster Green function. The cost function now can be written as

$$f_{cost} = i\Im\left((s_1)^{RK} - (s_2)^{RK}, (s_1)^{KA} - (s_2)^{KA}\right) \tag{3.29}$$

Note: R denotes the retarded part, K the Keldysh and A the advanced part of the function.
The minimum of the cost function has to be found for every value of E and the corresponding parameters t'_{cb} and ϵ_b saved. Theses parameters will then be used to calculate the Green function and with that the current at a certain value E.

3.3 Results and Analysis

The idea of this thesis was to use VCA on a finite one-dimensional tight-binding model and see if the altered self-energy due to an auxilary bath site leads to a different behaviour for values of $U \neq 0$. In particular, one goal was to see if metallic chains can be constructed for these values.
For $U = 0$ the auxilary bath should have no impact on the results. So the starting point is to look at

U = 0

Before the VCA parameters t'_{cb} and ϵ_b were calculated self-consistently, some values were set by hand to show that for the non-interacting case the results do not vary from the CPT results.

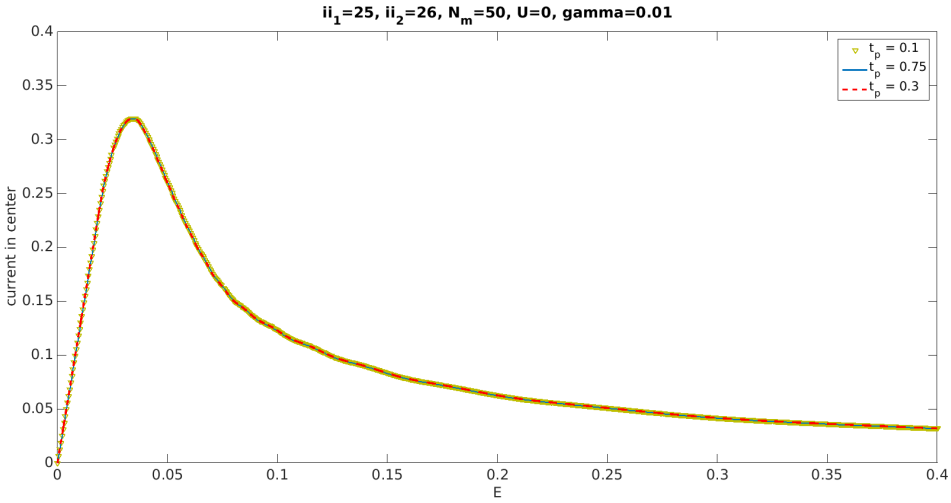

FIGURE 3.2: Different values of t'_{cb} for $U = 0$ give the same current curve. ϵ_b was set to 1.

For all three values of t'_{cb} (indicated as t_p in the figure) the current is the same as for the $U = 0$ result in the previous chapter. The bath has no influence on the current results for $U = 0$.

U = 1

Now that the program has been tested, it is possible to try to gain results for the interacting case. As the parameters have to be optimized for every value of electric field E the calculation time is quite intense. So the only system that could be calculated was a single physical site with the auxilary bath site and the fermionic heat bath, coupled to the leads.
The results for $U = 1$ are shown in this section. Before the current curve for this case is shown, it is interesting to discuss how the optimal VCA parameters are dependent on the electric field. For that reason the dependence is shown in the following figure.

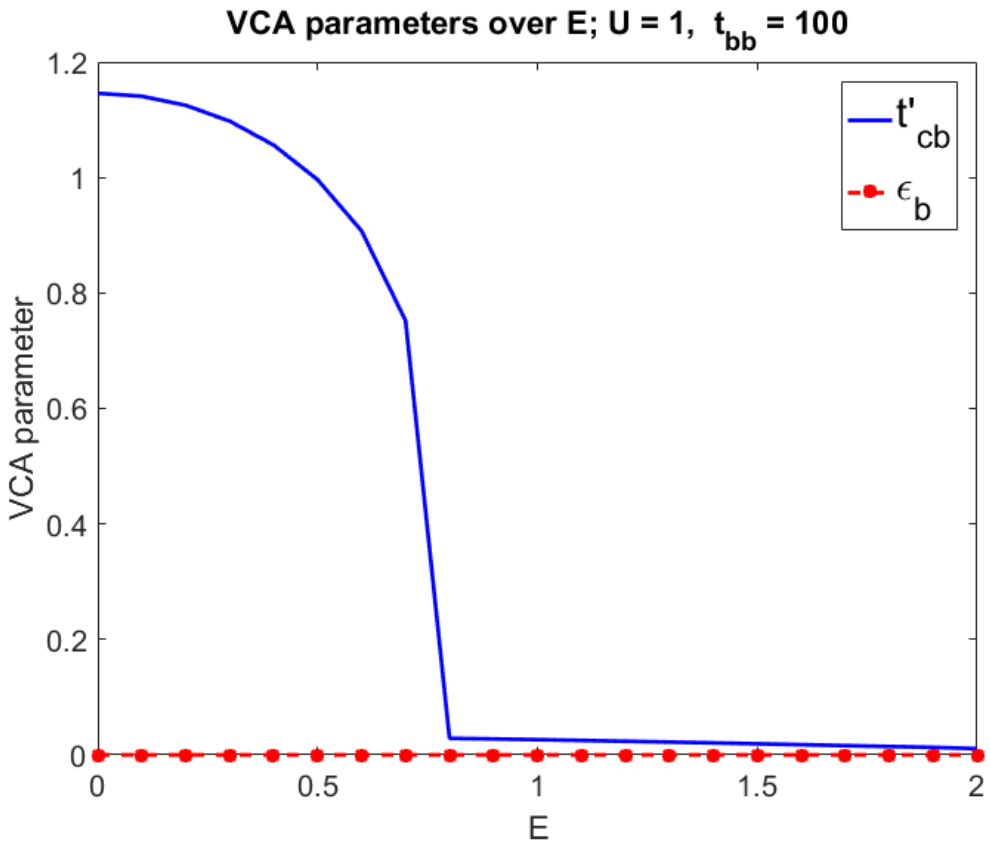

FIGURE 3.3: Dependence of the VCA parameters to the electric field.

The on-site energy of the auxilary bath ϵ_b is zero for all values of E. This is reasonable, because an on-site energy of zero corresponds to a half-filled band, which was taken as granted throughout the whole calculation.
Interesting is the behaviour of the hopping parameter into the auxilary bath t'_{cb}. For values of $E < 0.8$ the optimal parameter that was found self-consistently is in the range of $[1.2, 0.8]$. At $E = 0.8$ there is a jump and at values $E \geq 0.8$, the hopping parameter $t'_{cb} = 0$. This means that for values $E \geq 0.8$ the VCA results are the same as the plain CPT results.
So the VCA calculation corresponds to a phase-transition of the one-dimensional tight-binding Hubbard model.

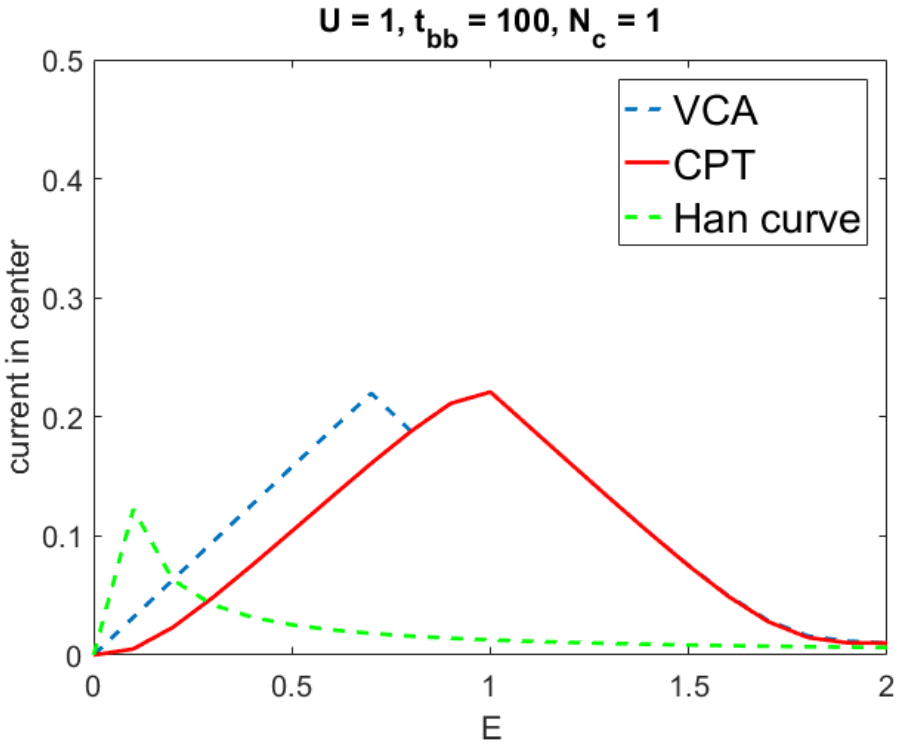

FIGURE 3.4: Current density for U = 1

In figure 3.4 the three different results for green: analytic solution, red: CPT result and blue: VCA result are shown.
At values $E \geq 0.8$ the VCA and CPT results overlap, as the hopping into the auxilary bath becomes zero. So the interesting part is for smaller values of E, where the chain showed a non-metallic behaviour in the CPT calculations. Lookig at figure 3.4 it is striking that the VCA curve does indeed show a metallic behaviour, with a less steep curve than the $U = 0$ results. It appears that the altered self-energy due to the auxilary bath place changes the behaviour of the tight-binding chain.
A calculation for a smaller hopping in the fermionic bath chains was done as well:

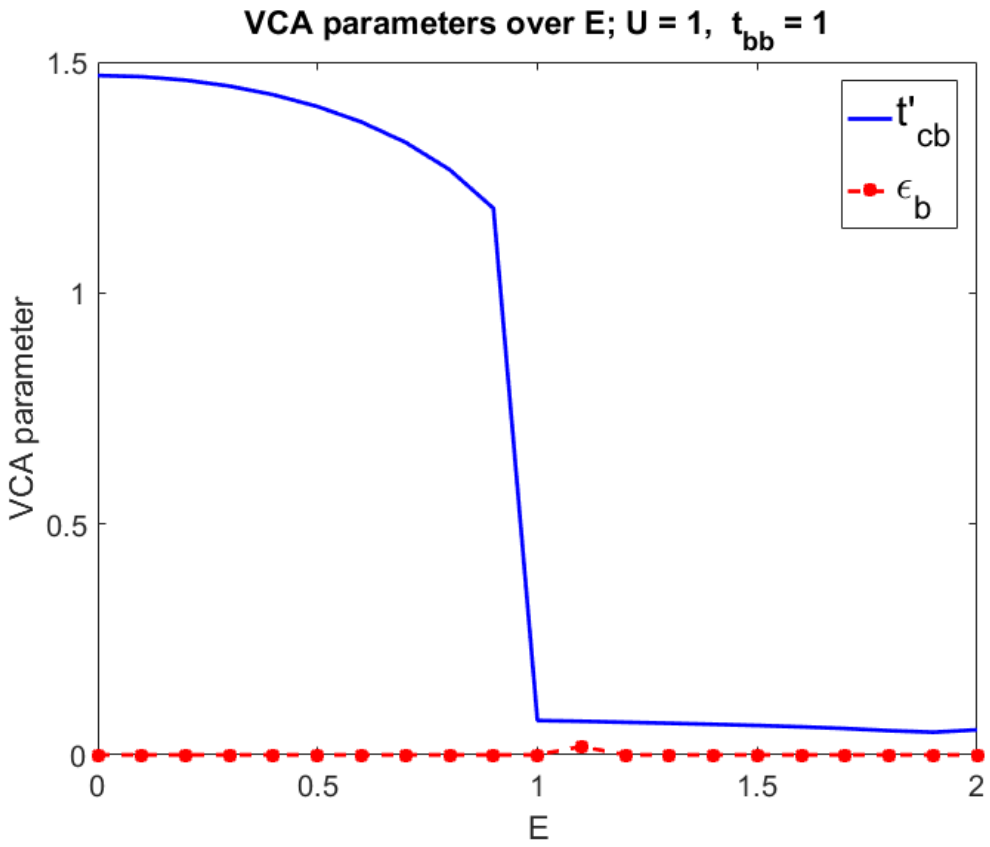

FIGURE 3.5: Dependence of the VCA parameters to the electric field.

Comparing these results to figure 3.3 it shows that the behaviour is nearly the same, but the jump, when the hopping parameter t'_{cb} becomes zero is at $E = 1$. The phase-transition occurs at a higher value of the external electric field.
One has to note that the jump to a non-zero value of the on-site energy ϵ_b is due to a convergence problem in the optimization process. For a smaller hopping inside the fermionic bath chain the on-site energy of the auxilary bath is zero at all values of E, but due to smaller energy-dissipations the critical value of E, where the phase-transition happens is shifted.

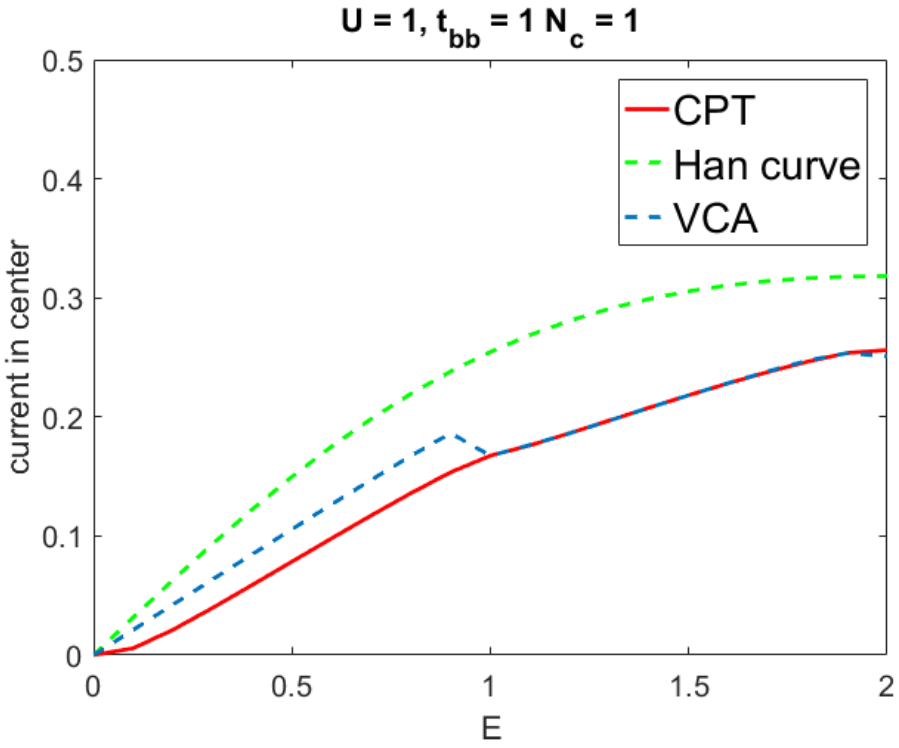

FIGURE 3.6: Current density for U = 1

U = 2

For values of $U = 2$ the VCA calculations were done as well. Keeping in mind the results from the 1-site cluster CPT calculations (depicted in fig. 2.10) the CPT calculations gave a rather damped current curve. The optimal VCA parameters were found and are shown in the following figure.

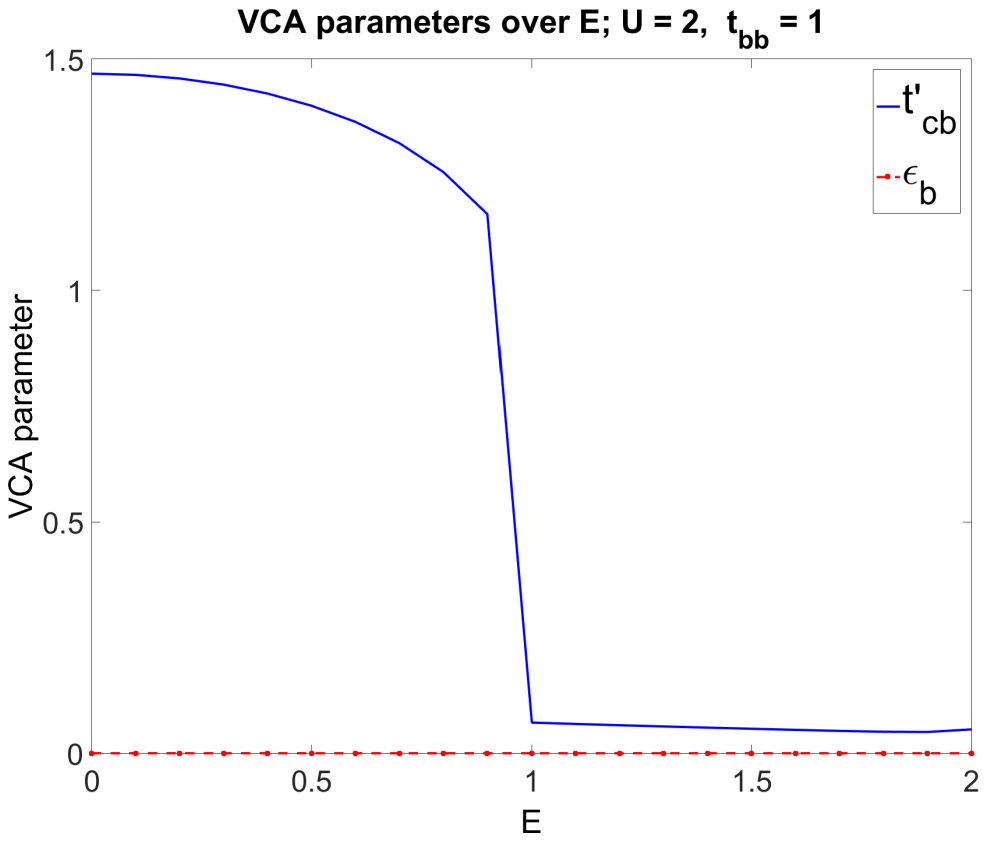

FIGURE 3.7: Dependence of the VCA parameters on the electric field.

The values of the parameters show a similar picture. The on-site energy is zero, while the hopping parameter starts at a value ≈ 1 and endures a jump to around zero at values of $E = 1$. Once again the hopping in the bath chain was set to $t_{bb} = 1$.

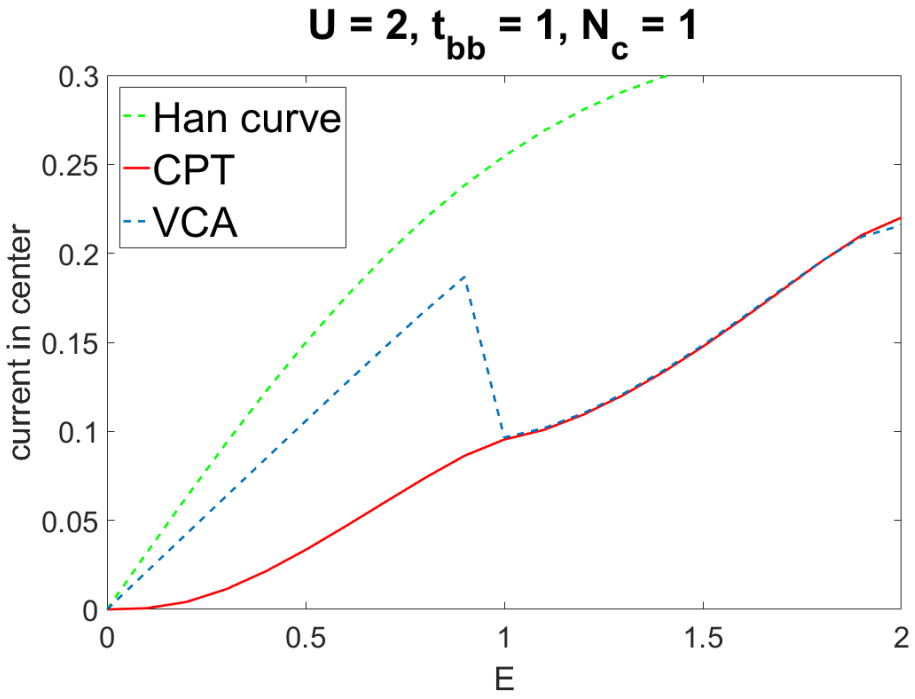

FIGURE 3.8: Current density for U = 2 and $t_{bb} = 1$

Looking at the current curve it is striking that the VCA result once again lies in between the CPT calculation and the analytical solution for $U = 0$ (i.e. Han curve in green). The VCA solution gives a linear, metallic response for values up to $E = 1$.
Also the VCA calculation for $t_{bb} = 100$ was done.

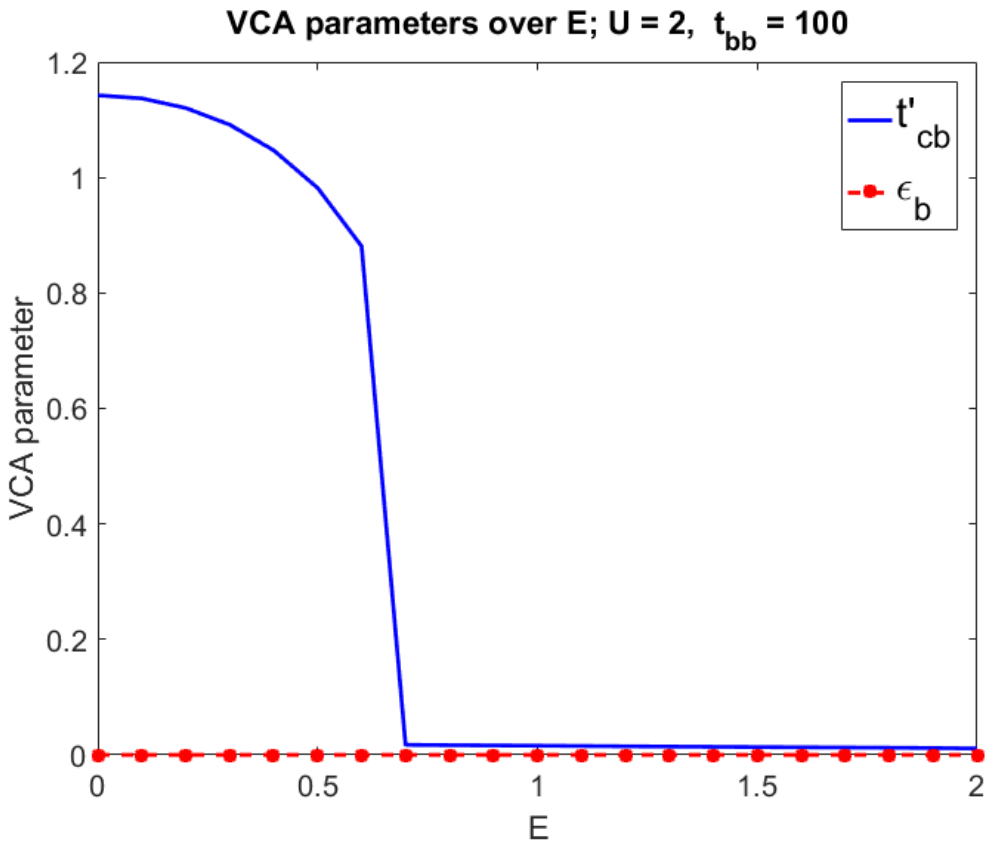

FIGURE 3.9: Dependence of the VCA parameters on the electric field.

Like for $U = 1$ the jump in the hopping strength t'_{cb} is at a lower value of E. Interesting is the current curve for this case.

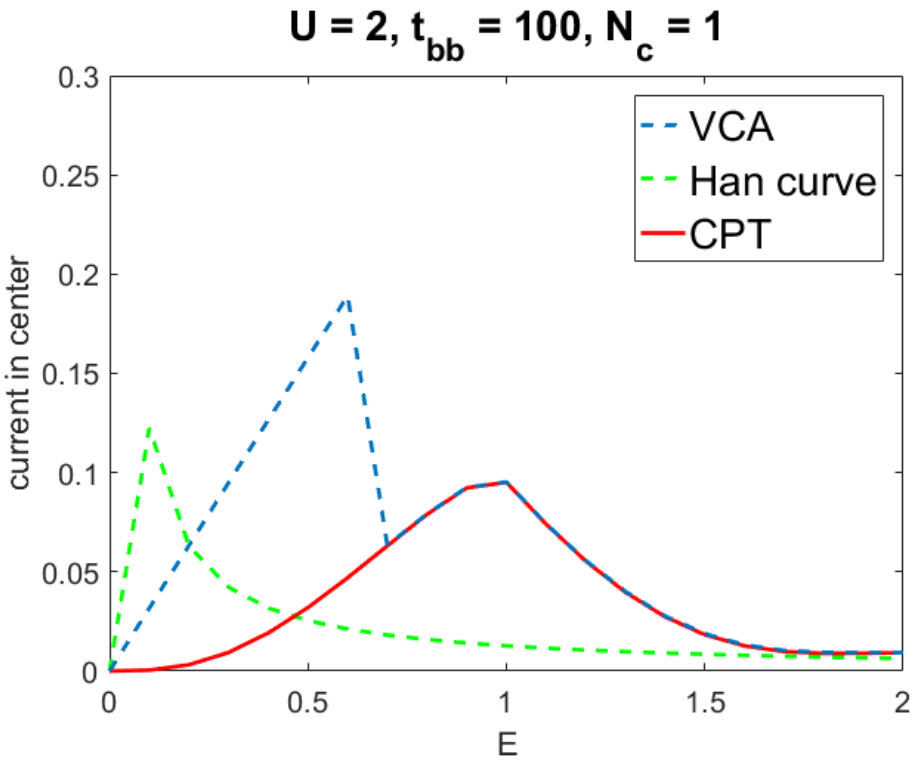

FIGURE 3.10: Current density for U = 2 and $t_{bb} = 100$

While the VCA again gives a linear response up until the value of E, where the hopping becomes zero, the current has a higher peak value, than the non-interacting analytical Han curve!
Summarizing it can be said, that the VCA method indeed achieves different results, compared to the plain CPT calculations. While the changing on-site energy does not play a role in the non-interacting case, for values $U \neq 0$ the behaviour changes drastically. With the method of VCA there occurs a phase-transition in the model. Of course it would be more interesting to make calculations for a longer chain and look at the results there but obtaining metallic results for the 1-site problem is an important and interesting start.

Chapter 4

Electronic transport through a quantum dot of spinless fermions

4.1 Introduction

Spinless fermions are, as the name already reveales, modeling particles that obey the same rules of fermions, as e.g. electrons, but are not assigned with a spin. Double occupations of sites are therefore forbidden, as two spinless fermions on one site cannot be discriminated by different internal quantum numbers. The spin-statistics theorem relates the spin of a particle to the particle statistics it obeys. [42] This follows naturally from the unification of quantum mechanics and special relativity, while a correlation between spin and statistics in non-relativistic quantum mechanics can be seen as an empirical law. [40] However the model of spinless fermions is a commonly used model e.g. to describe 3d electrons of the Fe^{2+} ions which all have the same spin direction because of strong ferrimagnetic ordering. [25]
In the last chapter of this thesis, spinless fermions are treated with CPT, motivated by the work of Christian Schiegg Michael Dzierzawa and Ulrich Eckern, who treated the same model with a Hartree-Fock approximation [36]. They state that the advantages of HF calculations lie within low computational costs and great flexibility with respect to dimensionality, system size and geometry as well as finite temperature and type and range of interactions. The goal of this work is to achieve comparable results with CPT. However it has to be noted that especially in terms of finite temperature CPT as it is used in this thesis the HF approach is more promising as only a temperature of zero will be used to calculate the necessary Green functions. Considering the numerical calculation time the CPT is a very fast method and the problem of having to find converged steady-state solutions from time evolutions will not be a problem, while HF results are vulnerable to mistakeably assumed converged steady-states.
The method will be similar to what has been done in chapter 2, with some small differences in terms of how the chemical potential will be treated when shifting Green functions in energy space as well as obviously a different model.

4.2 Model

Considered is a one-dimensional model of spinless fermions with N_c central sites with nearest neighbor interaction U. The central region is coupled to lead N_L on

the left and N_R to the right. The hopping parameter t_0 is the same inside the leads as well as in the central region. The leads are coupled to the central region with a weaker hopping parameter t'

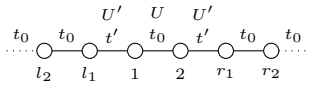

FIGURE 4.1: Model with N_c = 2. The leads are two semi-infinite tight-binding chains with hopping parameter t_0

The Hamiltonian for the central region reads as

$$\hat{H}_C = \sum_{i=1}^{2} \left\{ -t_0 \left(\hat{c}_i^\dagger \hat{c}_{i+1} + h.c. \right) + U \left(\hat{n}_i - \frac{1}{2} \right) \left(\hat{n}_{i+1} - \frac{1}{2} \right) \right\} \tag{4.1}$$

As there are only two sites in the central region an exact solution can be handily found by exact diagonalisation of the Hamilton-operator, which provides a 2x2 matrix.
The Hamiltonians for the coupling of the left lead to the center region as well as the coupling of the right lead to the center region read as

$$\hat{H}_{LC} = -t' \left(\hat{c}_{l_1}^\dagger \hat{c}_1 + h.c. \right) + U' \left(\hat{n}_{l_1} - \frac{1}{2} \right) \left(\hat{n}_1 - \frac{1}{2} \right) \tag{4.2}$$

$$\hat{H}_{CR} = -t' \left(\hat{c}_2^\dagger \hat{c}_{r_1} + h.c. \right) + U' \left(\hat{n}_2 - \frac{1}{2} \right) \left(\hat{n}_{r_1} - \frac{1}{2} \right) \tag{4.3}$$

Finally the Hamiltonians for the leads read as

$$\hat{H}_L = -t_0 \sum_{i=l_\infty}^{l_1} \left(\hat{c}_i^\dagger \hat{c}_{i+1} + h.c \right) \tag{4.4}$$

$$\hat{H}_R = -t_0 \sum_{i=r_1}^{r_\infty} \left(\hat{c}_i^\dagger \hat{c}_{i+1} + h.c \right) \tag{4.5}$$

The Hamiltonian for the full system then is

$$\hat{H} = \hat{H}_L + \hat{H}_{LC} + \hat{H}_C + \hat{H}_{CR} + \hat{H}_R \tag{4.6}$$

As the model shall be one of spinless fermions, there cannot occur any double occupied sites and the base vectors for the Fock-Space are

$$
\begin{aligned}
|\psi_0\rangle &= |00\rangle = |0\rangle \\
|\psi_1\rangle &= |10\rangle = \hat{c}_1^\dagger |0\rangle \\
|\psi_2\rangle &= |01\rangle = \hat{c}_2^\dagger |0\rangle \\
|\psi_3\rangle &= |11\rangle = \hat{c}_1^\dagger \hat{c}_2^\dagger |0\rangle
\end{aligned} \tag{4.7}
$$

with $|0\rangle$ being the vacuum state, giving a rather manageable Hamiltonian in this base:

$$
H = \begin{array}{c} \\ |\psi_0\rangle \\ |\psi_1\rangle \\ |\psi_2\rangle \\ |\psi_3\rangle \end{array}
\begin{array}{c}
\begin{array}{cccc} |\psi_0\rangle & |\psi_1\rangle & |\psi_2\rangle & |\psi_3\rangle \end{array} \\
\begin{pmatrix} \frac{U}{4} & 0 & 0 & 0 \\ 0 & \frac{-U}{4} & t_0 & 0 \\ 0 & t_0 & \frac{-U}{4} & 0 \\ 0 & 0 & 0 & \frac{U}{4} \end{pmatrix}
\end{array} \tag{4.8}
$$

4.3 Method

To obtain the Green Function of the isolated cluster (i.e. the quantum dot) g^0 the groundstate of the Hamiltonian φ_0 was found by ED and using the Lehmann representation of the Green function 1.19.
The Green function of the leads g^l and g^r was calculated using the formula for semi-infinite tight binding chains, eq. 2.12, with hopping strength t_0.
Via Dyson equation the quantum dot was coupled to the left and right lead, which gives for the advanced/retarded part:

$$
G_{a/r}^{-1}(\omega) = (g_{a/r}^0)^{-1} - M^l g_{a/r}^l M^r - M^r g_{a/r}^r M^l \tag{4.9}
$$

with the coupling matrices

$$
M^l = \begin{pmatrix} 0 & t' \\ 0 & 0 \end{pmatrix} \tag{4.10}
$$

and

$$
M^r = \begin{pmatrix} 0 & 0 \\ t' & 0 \end{pmatrix} \tag{4.11}
$$

This Green function can easily be inverted

$$
G_{a/r} = \left[G_{a(r}^{-1} \right]^{-1} \tag{4.12}
$$

For the Keldysh part the Dyson equation reads as:

$$
G_K^{-1} = -M^l g_K^l M^r - M^r g_K^r M^l \tag{4.13}
$$

and finally inverting

$$
G_K = -G_a G_K^{-1} G_r \tag{4.14}
$$

to obtain the Keldysh part of the Green function of the quantum dot, coupled to the left and right lead. Using eq. 1.76 the current through the quantum dot can be calculated from the Keldysh part of the Green function.
When calculating the Keldysh part of the lead Green function the chemical potential comes into play. For this chapter the current will not be induced by an electric field, but rather a bias V_B due to the difference in the chemical potential for the left and right lead is induced. For the analysis of the model the chemical potential was treated in two different ways:

1. Half-filled leads for all bias values. The chemical potential inside the leads stays at $\mu = V_B/2$
2. The chemical potential is shifted $\mu_{l/r} = \pm V_B/2$

FIGURE 4.2: The position of the chemical potential in the energy space is denoted by the red line. The band is half-filled in that case, meaning the chemical potential is fixed relative to band.

FIGURE 4.3: The chemical potential inside the leads is shifted. The bands are no longer half-filled at $V_B \neq 0$

Both methods to produce a bias voltage will be discussed and depicted in the next section. The applied method will be indicated.

4.4 Results

To compare the method of CPT on the model of spinless fermions the values of U were set to $1, -1, 0$ according to the results given in [36].

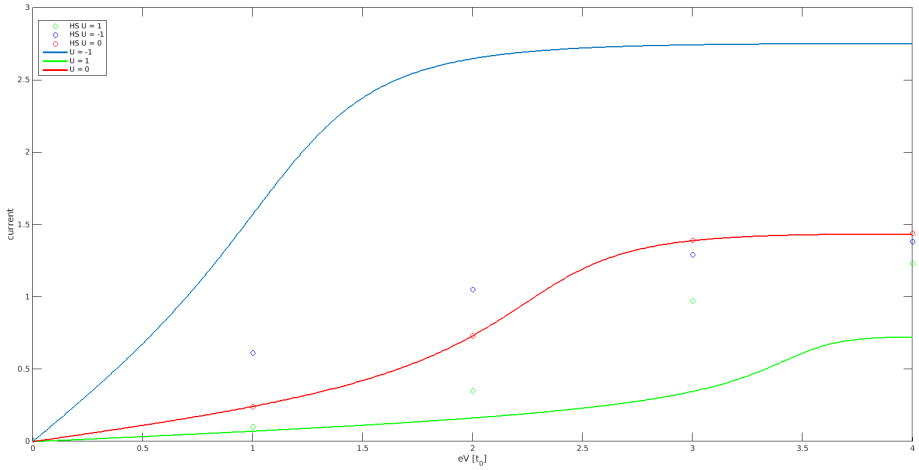

FIGURE 4.4: Current curve for the quantum dot for $t' = 0.5t_0$. The symbols are the data obtained from Hubbard-Stratonovich approach (taken from [36])

In the above figure a summary of the CPT results for the spinless fermions model is given. The symbols are the data taken from [36]. The values for $U = 0$ go through the points of the respective Hubbard-Stratonovich data, however the results for $U = 1$ and $U = -1$ are off. Not only are they far away from the results, of the other paper, but they are also qualitatively different. The $U = -1$ curve is above the $U = 0$ curve of the CPT approach, while for the Hubbard-Stratonovich approach the $U = 0$ curve starts underneath the $U = -1$ result, but crosses it at vaules $eV > 2$.
To compare the results with the Hartree-Fock approach, a figure from [36] is shown.

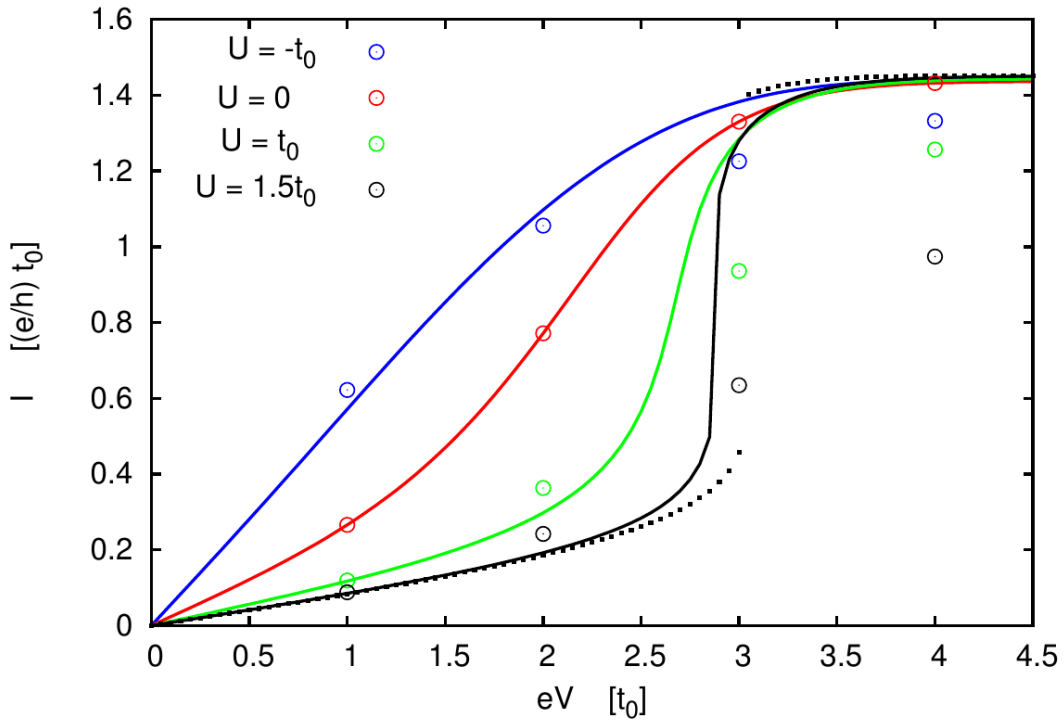

FIGURE 4.5: Results of the Hartree-Fock approximation (taken from [36])

It is striking that for the Hartree-Fock approach all the current curves converge onto the $U = 0$ curve. This is not the case for the CPT approach. However it is said in [36] that the collapse of the curves at larger values of eV is an artifact of the Hartree-Fock approach.
Note: All calculations have been done, shifting the chemical potential of the leads, as indicated in figure 4.3.
In the following the results for the case of a fixed chemical potential in the leads (figure 4.2) are shown.

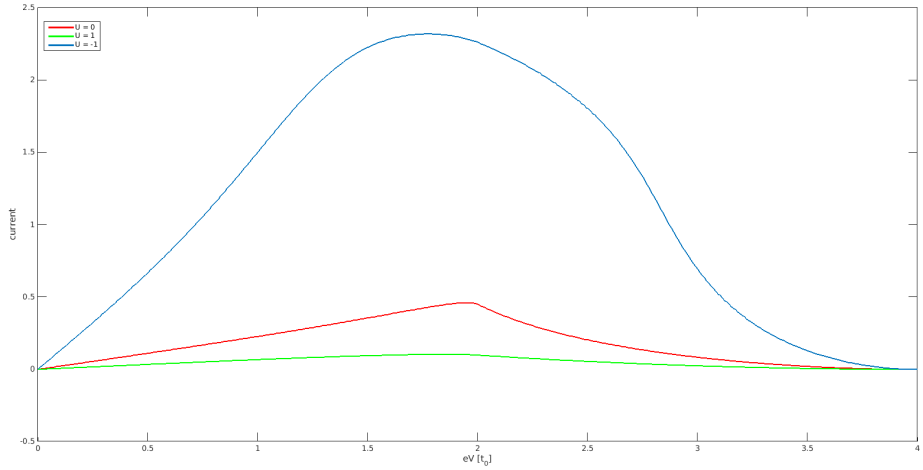

FIGURE 4.6: Current curve for the quantum dot for $t' = 0.5t_0$.

Keeping the chemical potential fixed in a way that the leads stay half filled at all values of eV is how it was treated in chapter 2. When shifting the leads in energy space there is a finite span of overlap. At a maximum overlap the current curves show a maximum and when the leads are shifted far enough apart there is no more overlap, i.e. a zero current at higher values of eV.
Shifting the chemical potential inside the leads gives a saturation current, when one lead is completely empty and the other one completely filled. The current does not change anymore, as there are always electrons in the left lead and none in the right.
Comparing figures 4.4 and 4.6 the order of the curves stays the same. The $U = -1$ curve shows the highest current, $U = 0$ is in the middle and $U = 1$ shows the lowest current.
With the method of CPT it was not possible to achieve results that fall on the Hubbard-Stratonovich data. An idea to further improve the method is to make use of a master equation approach [31]. In this work the ground state falls into a certain particle sector that either has zero, one, or two particles in it. The idea is to use a density matrix that combines all the particle sectors to form the ground state.

Chapter 5

Conclusion

This thesis deals with nonequilibrium calculations in finite tight-binding chains, with various cluster perturbation methods leading to the variational cluster approximation.
To get a feeling for the behaviour of finite tight-binding chains the cluster perturbation theory was used to calculate the current, due to an electric field. The chain was first devided into clusters of size 1 and later on into clusters of size 2. It was important to provide a proper dissipation mechanism to the system, therefore an semi-infinite tight-binding bath chain was coupled to every physical site of the chain.
The influence of the hopping strength inside those bath chains was analyzed. A bigger hopping parameter means a lower damping parameter which leads to a sharp peak in the current curve, while for a lower hopping parameter, the current density shows a broad curve, without much suppression. Furthermore the chain shows a metallic behaviour with a linear response for $U = 0$. This behaviour is changed to a semiconducting one for larger values of U. It was confirmed that the cluster size does indeed play a role, in terms of appearing short-range antiferromagnetic order.
Finally the variational cluster approximation was introduced. The idea is to make the self-energy depending on a set of parameters, that can be found self-consistently. In this particular thesis the VCA parameters were introduced by adding an auxilary bath place to each site of the chain. The hopping into that bath as well as the on-site energy are variational.
For the non-interacting case the results are independent on the VCA parameters. The results are always the same, as for the CPT calculations. However, when looking at values $U \neq 0$ the VCA calculation showed a difference to the CPT results. It was found that the onsite energy of the auxilary bath is close to zero for all inspected values of U. The hopping into the bath is around 1 for lower values of E and jumps down to zero. The jump is at $E = 1$ for a hopping parameter of $t_{bb} = 1$ inside the fermionic bath chain and at a lower value of E for a hopping $t_{bb} = 100$.
There is a linear response of the current in the lower energy field regime, making the chain metallic even at values $U \neq 0$. The system observed, however is only one physical site, coupled to an auxilary bath, the fermionic bath chain and two leads. Bigger system could not be calculated as the computation for this small system was considerably time-consuming.
The final chapter deals with spinless fermions, sitting on a quantum dot. The method of CPT was used to obtain a current curve, due to a bias voltage, driven

by different chemical potentials in the two leads. The results were compared with a Hartree-Fock approximation as well as a Hubbard-Stratonovich approach. However, it was not possible to achieve the same results as any of those calculations with a CPT approach. An idea was to use a master equation calculation to obtain density matrices for the ground state, and use those in the calculation of the Green function to do a CPT calculation.

Bibliography

[1] M. Aichhorn, E. Arrigoni, M. Potthoff, and W. Hanke. Variational cluster approach to the Hubbard model: Phase-separation tendency and finite-size effects. Phys. Rev. B, 74(23):235117, 2006.

[2] C. Aron, G. Kotliar, and C. Weber. Dimensional Crossover Driven by an Electric Field. Phys. Rev. Lett., 108(8):086401, 2012.

[3] R. Bersohn. Quantum Statistical Mechanics. Science, 139(3553):399–400, 1963.

[4] Felix Bloch. Über die Quantenmechanik der Elektronen in Kristallgittern. Zeitschrift für Physik, 52(7):555–600, 1929.

[5] Aldo Di Carlo, P. Vogl, and W. Pötz. Theory of Zener tunneling and Wannier-Stark states in semiconductors. Phys. Rev. B, 50:8358–8377, 1994.

[6] E.N. Economou. Green's Functions in Quantum Physics. Springer Series in Solid-State Sciences. Springer, 2006.

[7] J. Feldmann, K. Leo, J. Shah, D. A. B. Miller, J. E. Cunningham, T. Meier, G. von Plessen, A. Schulze, P. Thomas, and S. Schmitt-Rink. Optical investigation of Bloch oscillations in a semiconductor superlattice. Phys. Rev. B, 46:7252–7255, 1992.

[8] A.L. Fetter and J. D. Walecka. Quantum Theory of Many-Particle Systems. Dover Publications, Inc., 1991.

[9] J.O. Fjaerestad. Introduction to Green functions and many-body perturbation theory, 2013.

[10] M. Glück, A. R. Kolovsky, and H. J. Korsch. Wannier-Stark resonances in optical and semiconductor superlattices. Phys. Rep., 366:103–182, 2002.

[11] Vincenzo Grecchi, Marco Maioli, and Andrea Sacchetti. Stark resonances in disordered systems. Comm. Math. Phys., 146(2):231–240, 1992.

[12] Vincenzo Grecchi, Marco Maioli, and Andrea Sacchetti. Stark ladders of resonances: Wannier ladders and perturbation theory. Comm. Math. Phys., 159(3):605–618, 1994.

[13] Jong E. Han. Solution of electric-field-driven tight-binding lattice coupled to fermion reservoirs. Phys. Rev. B, 87:085119, 2013.

[14] T Hartmann, F Keck, H J Korsch, and S Mossmann. Dynamics of Bloch oscillations. New J. Phys., 6(1):2, 2004.

[15] H. Haug and A.P. Jauho. Quantum Kinetics in Transport and Optics of Semiconductors. Springer Berlin Heidelberg, 1998.

[16] M. H. Hettler, A. N. Tahvildar-Zadeh, M. Jarrell, T. Pruschke, and H. R. Krishnamurthy. Nonlocal dynamical correlations of strongly interacting electron systems. Phys. Rev. B, 58:R7475–R7479, 1998.

[17] A. P. Jauho. Introduction to the keldysh nonequilibrium green function technique, 2006.

[18] L. V. Keldysh. Diagram technique for nonequilibrium processes. Sov. Phys. JETP, 20:1018, 1965.

[19] M. Knap, W. von der Linden, and E. Arrigoni. Nonequilibrium steady state for strongly correlated many-body systems: Variational cluster approach. Phys. Rev. B, 84(11):115145, 2011.

[20] Gabriel Kotliar, Sergej Y. Savrasov, Gunnar Pálsson, and Giulio Biroli. Cellular dynamical mean field approach to strongly correlated systems. Phys. Rev. Lett., 87:186401, 2001.

[21] E. Kozik, M. Ferrero, and A. Georges. Nonexistence of the luttinger-ward functional and misleading convergence of skeleton diagrammatic series for hubbard-like models. Phys. Rev. Lett., 114(15):156402, 2015.

[22] H. Lehmann. über eigenschaften von ausbreitungsfunktionen und renormierungskonstanten quantisierter felder. Il Nuovo Cimento, 11(4):342–357, 1954.

[23] J. Li, C. Aron, G. Kotliar, and J. E. Han. Electric-field-driven resistive switching in the dissipative hubbard model. Phys. Rev. Lett., 114(22):226403, 2015.

[24] A. I. Lichtenstein and M. I. Katsnelson. Antiferromagnetism and d-wave superconductivity in cuprates: A cluster dynamical mean-field theory. Phys. Rev. B, 62:R9283–R9286, 2000.

[25] B. Lorenz. Charge order in the spinless fermion model. physica status solidi (b), 101(1):297–302, 1980.

[26] Thomas Maier, Mark Jarrell, Thomas Pruschke, and Matthias H. Hettler. Quantum cluster theories. Rev. Mod. Phys., 77:1027–1080, 2005.

[27] J.W. Negele and H. Orland. Quantum Many-particle Systems. Westview Press, 1998.

[28] J. Neumayer, E. Arrigoni, M. Aichhorn, and W. von der Linden. Current characteristics of a one-dimensional hubbard chain: Role of correlation and dissipation. Phys. Rev. B, 92(12):125149, 2015.

[29] Jakob Neumayer. Equilibrium and transport properties of single-layer graphene nanoribbons. Master's thesis, TU Graz, 2014.

[30] Wolfgang Nolting. Grundkurs Theoretische Physik 7. Springer Verlag, 2009.

[31] Martin Nuss, Gerhard Dorn, Antonius Dorda, Wolfgang von der Linden, and Enrico Arrigoni. Master equation based steady-state cluster perturbation theory. Master equation based steady-state cluster perturbation theory, 2015.

[32] M. Potthoff. Self-energy-functional approach to systems of correlated electrons. Eur. Phys. J. B, 32(4):429–436, 2003.

[33] M. Potthoff. Dynamical variational principles for strongly correlated electron systems. In B. Kramer, editor, Advances in Solid State Physics, volume 45 of Advances in Solid State Physics, page 135, 2006.

[34] J. Rammer and H. Smith. Quantum field-theoretical methods in transport theory of metals. Rev. Mod. Phys., 58:323–359, 1986.

[35] A. Sacchetti. Existence of the Stark-Wannier quantum resonances. Journal of Mathematical Physics, 55(12):122104, December 2014.

[36] C. Schiegg, M. Dzierzawa, and U. Eckern. Non-equilibrium transport through a model quantum dot: Hartree-fock approximation and beyond. New J. Phys., 17(8):083060, 2015.

[37] D. Senchal, D. Perez, and M. Pioro-Ladrire. Spectral weight of the hubbard model through cluster perturbation theory. Phys. Rev. Lett., 84:522–525, 2000.

[38] D. Senechal. An introduction to quantum cluster methods, 2008.

[39] D. Senechal, D. Perez, and D. Plouffe. Cluster perturbation theory for hubbard models. Phys. Rev. B, 66(7):075129, 2002.

[40] Ben Simons. Identical particles — lecture notes, 2009. [Online; accessed 09-November-2016].

[41] Naoto Tsuji, Takashi Oka, and Hideo Aoki. Nonequilibrium steady state of photoexcited correlated electrons in the presence of dissipation. Phys. Rev. Lett., 103:047403, 2009.

[42] Wikipedia. Spin-statistics theorem — Wikipedia, the free encyclopedia, 2016. [Online; accessed 09-November-2016].

[43] Clarence Zener. A theory of the electrical breakdown of solid dielectrics. Proc. Roy. Soc. A, 145(855):523–529, 1934.